catalysts

MDPI

Review

Emission Control of Toluene in Iron Ore Sintering Using Catalytic Oxidation Technology: A Critical Review

Qiqi Shi [1,2], Dongrui Kang [1,2], Yuting Wang [1,2] and Xiao Zhang [1,2,*]

[1] Tianjin Key Laboratory of Clean Energy and Pollution Control, Hebei University of Technology, Tianjin 300401, China
[2] School of Energy and Environmental Engineering, Hebei University of Technology, Tianjin 300401, China
* Correspondence: zhangxiao@hebut.edu.cn

Abstract: Iron ore sintering flue gas containing large amounts of volatile organic compounds (VOCs) can form secondary photochemical smog and organic aerosols, thus posing a serious threat to human health and the ecological environment. Catalytic combustion technology has been considered as one of the most prospective strategies for VOC elimination. This paper focuses on a review of studies on catalytic removal of typical VOCs (toluene) on transition metal oxide catalysts in recent years, with advances in single metal oxides, multi-oxide composites, and supported metal oxide catalysts. Firstly, the catalytic activities of a series of catalysts for toluene degradation are evaluated and compared, leading to an analysis of the key catalytic indicators that significantly affect the efficiency of toluene degradation. Secondly, the reaction pathway and mechanism of toluene degradation are systematically introduced. Considering the site space and investment cost, the conversion of VOC pollutants to harmless substances using existing selective catalytic reduction (SCR) systems has been studied with considerable effort. Based on the current development of simultaneous multi-pollutant elimination technology, the interaction mechanism between the NH_3-SCR reaction and toluene catalytic oxidation on the surface is discussed in detail. Finally, views on the key scientific issues and the challenges faced, as well as an outlook for the future, are presented. This overview is expected to provide a guide for the design and industrial application of NO/VOC simultaneous removal catalysts.

Keywords: flue gas; VOCs; NO; simultaneous elimination; interaction mechanism

Citation: Shi, Q.; Kang, D.; Wang, Y.; Zhang, X. Emission Control of Toluene in Iron Ore Sintering Using Catalytic Oxidation Technology: A Critical Review. *Catalysts* **2023**, *13*, 429. https://doi.org/10.3390/catal13020429

Academic Editor: Wenpo Shan

Received: 19 January 2023
Revised: 9 February 2023
Accepted: 15 February 2023
Published: 16 February 2023

1. Introduction

In recent years, the pattern of air pollution in China has undergone profound changes, and the combination of PM 2.5 and ozone (O_3) pollution has become an important air pollutant affecting urban and regional air quality in China [1]. PM 2.5 and O_3 can result in respiratory/cardiovascular diseases and pose a great risk to human health. Since the implementation of China's air pollution prevention and control action plan, PM 2.5 pollution has been improved, but O_3 pollution is still deteriorating and has become an important exceedance pollutant. It has been reported that ozone concentrations in China continued to increase during 2013–2019 [2]. VOCs are a variety of organic compounds with boiling points of 50 °C to 260 °C at room temperature. Many VOCs are highly toxic, diffusible, and volatile and are released into the environmental matrix as important precursors of PM 2.5 and O_3. This leads to urban haze and photochemical smog, and therefore it is considered as a key factor in PM 2.5 and O_3 pollution.

Given the worsening environmental risks, the Chinese government implemented a multi-pronged approach to monitor VOC emissions from many enterprises and put in place many control measures. In the 14th Five-Year Plan, China has committed to decreasing VOC emissions by at least 10% in 2025 compared to 2020 and to achieving an emission control level that is basically at the international advanced level. In 2020, the Ministry of

Ecology and Environment of the People's Republic of China revised the air pollution evaluation index from "SO_2 and NO_x" to "VOC and NO_x". VOCs are primarily released from industrial production processes, solvent use, transportation, and fuel combustion [3]. As various industrial pollutant abatement measures are being implemented, the contribution of energy-intensive industries to VOC emissions should not be underestimated. In China, VOC emissions from combustion sources (excluding biomass combustion) are estimated to account for 7.4–10.4% of VOC emissions from all anthropogenic sources [4–6]. With government efforts, most primary pollutants concentrations have been significantly decreased [2]. These include the use of new energy vehicles to control mobile source pollutant emissions [7], the use of biomass or carbonized biomass with a lower environmental burden to partially replace coal to produce coke [8], and the development of catalytic oxidation technology to reduce VOC emissions in coal-fired power plants [9]. For the iron and steel industry, the VOC emissions from iron sintering process have also raised some special concerns. In China, the annual production of sintered ore can reach 1 billion tons/year, and more than 60 million tons of fossil fuels (coal, coke, natural gas, and oily sludge, etc.) are consumed in these steel plants [10]. The iron ore sintering process results in significant VOC emissions owing to the mixed combustion of fossil fuels, iron ore, and coke [10]. Especially in typical iron- and steel-producing cities such as Tangshan and Handan, iron ore sintering processes account for 18.7–30.0% of the national VOC emissions [11,12]. In response to the large VOC emissions from iron ore sintering plants, legislation has been introduced in China to regulate VOC emissions in the iron and steel industry. However, the actual industrial control technology is still in the initial stage. Li et al. [13] reported the VOC emission profiles in the iron ore sintering process, comparing sintering tanks and sintering simulation tests to determine VOC species and their concentrations. Wang et al. [10] explored the mechanisms and patterns of VOC emissions in iron ore sintering flue gas and critically discussed the feasibility of source control, process control, end-of-pipe control, and industrial VOC emission control technologies to treat sintering flue gas. Qian et al. [14] also systematically investigated the mechanism of PCDD/Fs generation in the iron ore sintering process and summarized new advances and technologies for PCDD/Fs emission reduction in terms of source, process, and end-of-pipe treatment. In these reviews, it is widely agreed that catalytic oxidation-based technology is one of the most effective methods to control emissions of VOCs, which can be converted to harmless CO_2 and H_2O as end products at low temperatures. However, a detailed exploration of catalytic oxidation control technologies and a review of key catalysts are still lacking based on the available iron ore emission characteristics.

NO as a precursor to ozone is also widely present in iron sintering flue gases. Selective catalytic reduction (SCR), a well-established reaction for NO elimination from such flue gases, has a process temperature range similar to that of catalytic oxidation technology. In recent years, the Chinese government has promoted the development of multi-pollutant synergistic control technologies to reduce the emissions of VOCs and NO_x [1]. However, in iron sintering flue gas emission control, SCR technology is usually used for single NO_x pollutant removal from flue gas. Installing separate end-of-pipe treatment units for VOCs in the same stationary emission source would occupy a large amount of site space, resulting in a complex process with large and costly systems [15]. Therefore, instead of building redundant facilities, the existing equipment can be fully utilized to remove both VOCs and NO in one catalytic system, which is a reasonable and cost-effective option. It can be seen that studying the synergistic removal of multiple pollutants under complex flue gas conditions is an inevitable trend in the development of industrial flue gas cleaning technology. However, feasible ways aiming at simultaneous multi-pollutant removal by SCR reactors in existing sinter flue gas cleaning technologies have not been identified. The recent research about the oxidation process of VOCs alone and its oxidation path and the synergistic mechanism of SCR + VOC catalytic oxidation still lacks a systematic review.

Therefore, this paper reviews the catalytic oxidation of VOCs over various transition metal oxides based on the emission characteristics of iron ore sintering processes to better

understand the removal of VOCs and to determine whether they can be applied in practical areas. In addition, we focus on an overview of the oxidation path of toluene degradation over non-homogeneous catalysts and the key factors affecting catalyst performance. In summary, this comprehensive review focuses on the relationships between catalyst performance, behavior, and the principles of catalytic oxidation of VOCs. The tasks of the review are to guide the design of more effective catalytic materials for VOC oxidation, to support the development of new technologies for the synergistic removal of multiple pollutants, and to provide a reference point to benefit designers, researchers, and managers by providing a useful resource for advancing VOC removal methods.

2. Emission Characteristics and Terminal Treatment

In a conventional iron ore sintering system (Figure 1a), sintering is carried out with iron ore fines and white ash fines as uncooked substances and coal fines and coke as fuels. After ignition, the sintered material layers undergo different treatment processes in sequence. The granular sintered material is transported into the sintering machine, where the surface of the sintered material is ignited by the vertical airflow and sintered from top to bottom [16]. The VOCs are generated in the low-temperature region without passing through the high-temperature region and are all volatilized into the sintering flue gas, thus resulting in VOC emissions. In addition, another significant contributor to VOC emissions is the presence of a micro-reducing environment surrounding some of the fuel inside the dense "sintered raw material pellet" during the sintering process. Hebei Province and the neighboring areas have the highest concentration of VOC emissions from the iron and steel industries. There are significant differences in VOC emission types and concentrations from distinct steel plants owing to coal type, raw materials, operating parameters of the sintering process, and significant differences in end-of-pipe treatment. Wang et al. [17] reported that samples were collected from sintering and pollution source processes in 2020 for high-energy-consumption industries in Hebei Province. It was found that in the steel industry (Figure 1b), alkanes were the most prevalent VOC species in the steel industry's sinter flue gas with SCR denitrification equipment installed, making up 45.9% of the total VOCs. Olefins were in second place with 27.3%, followed by aromatics (17.4%), halogenated hydrocarbons (6.8%), and oxygenated VOCs (2.5%). The best way to reduce VOC emissions without compromising iron ore sinter production goals is flue gas end-treatment technology, which can also handle the possible risk of sinter air pollutants. The attractive emission reduction efficiency achieved by flue gas end-treatment technology is highly tied to the emission characteristics of sinter flue gas, which include a high flow rate, low temperature, and low concentration. The VOCs generally have no recovery value, and catalytic oxidation in the presence of oxygen can decompose them completely, which has the advantages of high capacity and good real-time performance for VOC removal [18]. An important consideration in catalytic combustion technology is the choice of an appropriate catalyst. Catalytic combustion is a deep oxidation process in which reactive oxygen species break down chemical bonds, including the C-H and C-C bonds in VOCs [19]. The ideal active element in the catalyst must have strong redox properties to accelerate oxidative VOC degradation. It has been demonstrated that there is a relationship between the oxidizability of VOCs and their molecular weights. VOCs with higher molecular weights are expected to have more challenging degradation processes and higher activation energies [20]. Therefore, in this paper, toluene, as the most common aromatic and a pollutant difficult to degrade in iron sintering flue gas, is the subject of the pollutant review.

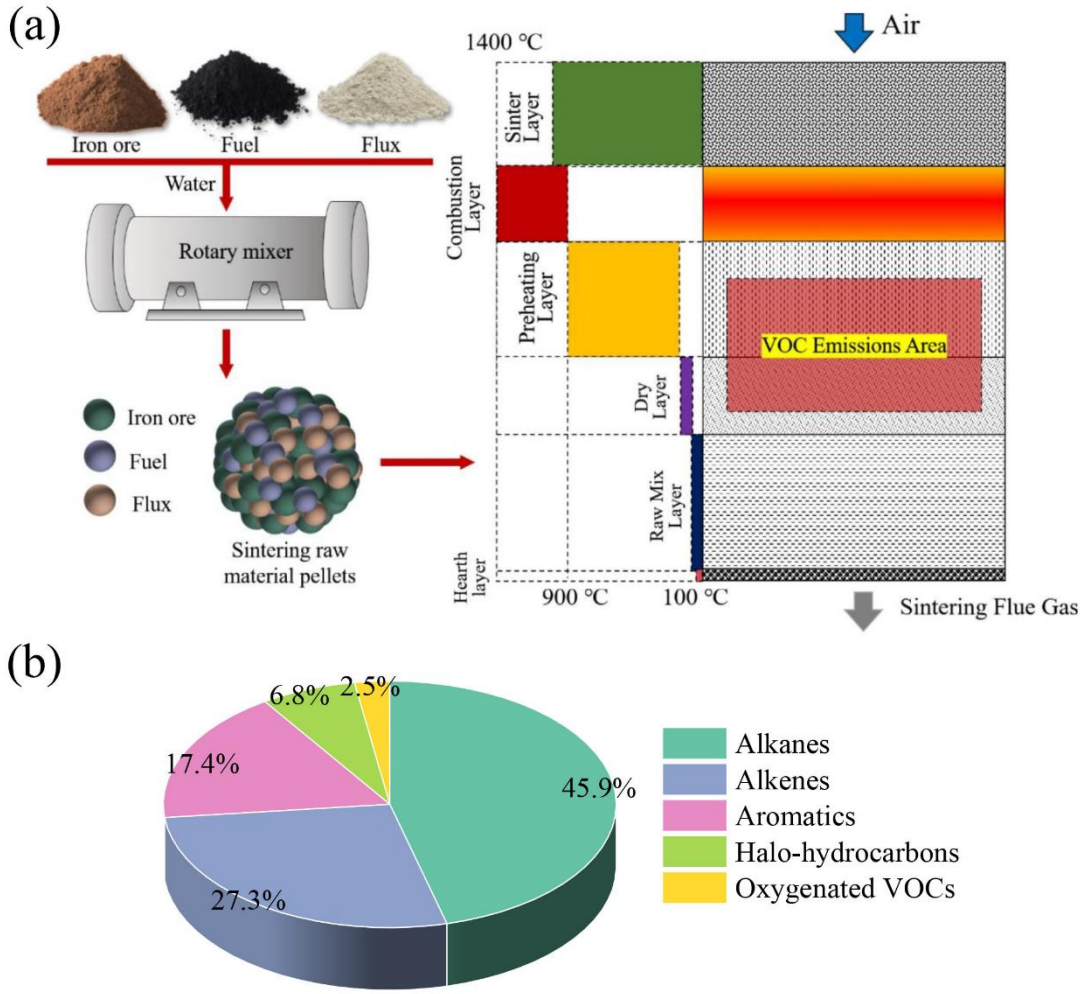

Figure 1. (**a**) Multilayer temperature distribution and VOC emission regions in sintered flue gas [10], Copyright 2022, Elsevier B.V. (**b**) Emission characteristics of different types of VOCs [17].

3. Transition Metal Oxide Catalysts for Toluene Purification

Many catalysts have been shown to be reactive for toluene oxidation. Noble metal oxides (Pt, Ag, Pb, etc.) and transition metal oxides (Mn, Co, Fe, Cu, Ce, etc.) are the most common catalysts. Among them, noble metal oxide catalysts have remarkable catalytic activity and stability, while the high price of precious metals leads to high industrial application costs and improper use can easily lead to catalyst poisoning [21]. In contrast, transition metal oxide catalysts are regarded as the best for catalyzing the removal of toluene due to their affordability, high catalytic activity, high selectivity, and robust tolerance to poisoning. The use of single [22–38] or multiple combinations of transition metal oxides has been widely reported. Here, the catalytic characteristics of the catalysts are summarized by dividing them into three categories: single metal oxides, multi-oxide composites, and supported metal oxide catalysts.

3.1. Single Metal Oxides

3.1.1. Manganese Oxides

MnO_x catalysts, with their low cost, high catalytic activity, and stability, show great potential for catalytic oxidation of VOCs and are recognized as the most competitive alternative to noble metal catalysts in the low-temperature region [39]. In general, the catalytic ability of MnO_x prepared by different methods is mainly influenced by numerous factors such as valence changes, crystal structure, exposed crystal surfaces, and microscopic morphology. These factors affect the catalytic activity of VOC abatement to some extent, as

shown in Table 1. Mn has various oxidation states, such as +2, +3, and +4, and MnO_x has different values of x due to the different oxidation states of manganese. The formation of various kinds of manganese oxides reflects the various valence states. Due to the different intrinsic properties, the catalytic oxidation activity of these MnO_x towards toluene is also different. Piumetti et al. [22] prepared mesoporous Mn_2O_3, Mn_3O_4, and Mn_xO_y (mixture of Mn_2O_3 and MnO_2) catalysts by solution combustion synthesis and evaluated their catalytic abilities for toluene oxidation. The results indicated that Mn_3O_4 exhibited excellent catalytic activity with 90% conversion at 248 °C because of the highest surface electrophilic oxygen content. Different crystal structures of MnO_2 in the same fraction (Figure 2) can affect the degree of active site exposure, resulting in different catalytic performances. Li et al. [23] explored the catalytic degradation of toluene over different phase structures of MnO_2, including β-, α-, γ-, and δ-MnO_2, showing that the catalytic activity followed the sequence of β- < α- < γ- < δ-MnO_2. The different crystal facets (Figure 2) of the exposed metal oxides confer special physicochemical properties to the functional materials, which are also closely related to their catalytic activity. Huang et al. [24] compared the toluene oxidation performance over α-MnO_2 catalysts with (110), (210), and (310) crystal facets. The α-MnO_2 with exposed (210) crystal facet catalysts exhibited the best catalytic performance and achieved complete toluene conversion at 140 °C. Chen et al. [25] prepared a series of α-MnO_2 catalysts by tuning the precipitation temperature in the redox precipitation process. The α-MnO_2-60 greatly enhanced the catalytic efficiency (T_{90} = 203 °C) and provided excellent H_2O resistance in toluene oxidation, which was mainly attributed to a large number of surface oxygen vacancies. The various morphologies of the MnO_x materials, including cubes, sheets, tubes, rods, and spheres, provide catalysts with unique characteristics that have an impact on the toluene degradation. Wang et al. [26] prepared nanorod, nanowire, and nanotube α-MnO_2 and nanoflower spherical Mn_2O_3 by hydrothermal and CCl_4 solution methods, respectively. The catalytic activities of these materials for toluene degradation were in the following order: nanorod α-MnO_2 > nanotube α-MnO_2 > nanoflower Mn_2O_3 > nanowire α-MnO_2, which was mainly caused by the differences in low-temperature reducibility, oxygen species concentration, and specific surface area. Moreover, the preparation conditions such as different types of Mn precursors and precipitating agents during the preparation process also affect the catalytic performance of toluene degradation to some extent. Lyu et al. [27] explored the catalytic activity of MnO_2 prepared from four Mn (II) precursors. The catalytic activity of these materials for toluene degradation followed the order of MnO_2-manganese acetate > MnO_2-manganese nitrate > MnO_2-manganese chloride > MnO_2-manganese sulfate. Zhang et al. [28] synthesized a series of MnO_x for the catalytic oxidation of toluene using four different precipitants. The results showed that Mn-$(NH_4)_2CO_3$ (T_{90} = 260 °C) had better catalytic efficiency than Mn-Na_2CO_3 (T_{90} = 281 °C), Mn-NaOH (T_{90} = 326 °C), and Mn-$NH_3 \cdot H_2O$ (T_{90} = 331 °C).

Table 1. Catalytic activity for toluene combustion over single metal oxides reported in the recent literature.

Catalysts	Synthesis Method	Toluene Concentration	WHSV or GHSV ($mL \cdot g^{-1} \cdot h^{-1}$ or h^{-1})	Activity T_{90} (°C)	Ref.
Mn_3O_4	Solution combustion synthesis	1000 ppm	19,100 h^{-1}	250	[22]
Mn_2O_3				268	
Mn_xO_y				291	
δ-MnO_2	Hydrothermal process	1000 $mg \cdot m^{-3}$	36,000 $mL \cdot g^{-1} \cdot h^{-1}$	233	[23]
γ-MnO_2				283	
α-MnO_2				309	
β-MnO_2				325	
α-MnO_2 (1 1 0)	Hydrothermal method	500 ppm	15,000 $mL \cdot g^{-1} \cdot h^{-1}$	109	[24]
α-MnO_2 (3 1 0)				170	
α-MnO_2 (2 1 0)				170	
α-MnO_2-60	Redox precipitation	1000 ppm	30,000 h^{-1}	203	[25]
Rod-like α-MnO_2	Hydrothermal or solution method	1000 ppm	20,000 $mL \cdot g^{-1} \cdot h^{-1}$	225	[26]
Tube-like α-MnO_2				233	
Flower-like Mn_2O_3				238	
Wire-like α-MnO_2				245	
MnO_2-manganese acetate	Redox reaction method	1000 ppm	90,000 $mL \cdot g^{-1} \cdot h^{-1}$	200	[27]
MnO_2-manganese nitrate				210	
MnO_2-manganese chloride				225	
MnO_2-manganese sulfate				236	
MnO_x-$(NH_4)_2CO_3$	Co-precipitation	500 ppm	60,000 $mL \cdot g^{-1} \cdot h^{-1}$	260	[28]
Mn-Na_2CO_3				281	
Mn-NaOH				326	
Mn-$NH_3 \cdot H_2O$				331	
CeO_2 microspheres	Polymer-modified hydrothermal method	1000 ppm	60,000 $mL \cdot g^{-1} \cdot h^{-1}$	210	[29]
CeO_2 hollow spheres	Hydrothermal method	1000 ppm	48,000 $mL \cdot g^{-1} \cdot h^{-1}$	207	[30]
CeO_2 nanorods				239	
CeO_2 cubes				296	
CeO_2 nanopolyhedra	Hydrothermal method	1000 ppm	24,000 $mL \cdot g^{-1} \cdot h^{-1}$	394	[31]
CeO_2 nanorods				400	
CeO_2 nanocubes				>400	
CeO_2 nanobelt	Conducted electrospinning	100 ppm	60,000 $mL \cdot g^{-1} \cdot h^{-1}$	230	[32]
CeO_2 nanotube				255	
CeO_2 wire-in-nanotube				345	
CeO_2-MOF	Sacrificial precursor	1000 ppm	20,000 $mL \cdot g^{-1} \cdot h^{-1}$	223	[33]
1D-Co_3O_4-nanoneedle	Hydrothermal method	1000 ppm	48,000 $mL \cdot g^{-1} \cdot h^{-1}$	257	[34]
2D-Co_3O_4-nanoplate				249	
3D-Co_3O_4-nanoflower				238	
Cube-stacked Co_3O_4 microspheres	Hydrothermal method	1000 ppm	48,000 $mL \cdot g^{-1} \cdot h^{-1}$	248	[35]
Plate-stacked Co_3O_4 flower				254	
Needle-stacked Co_3O_4 two-spheres				259	
Sheet-stacked fan-shaped Co_3O_4				>260	
NH/Am-Co_3O_4	ZIF template induction	3000 ppm	30,000 $mL \cdot g^{-1} \cdot h^{-1}$	220	[36]
Hollow Co_3O_4 polyhedron	ZIF-67 template	12,000 ppm	21,000 $mL \cdot g^{-1} \cdot h^{-1}$	258	[37]
ZSA-1 Co_3O_4	Co-MOFs template	-	20,000 $mL \cdot g^{-1} \cdot h^{-1}$	240	[38]

T_{90}: the temperature at which conversion efficiency reaches 90%.

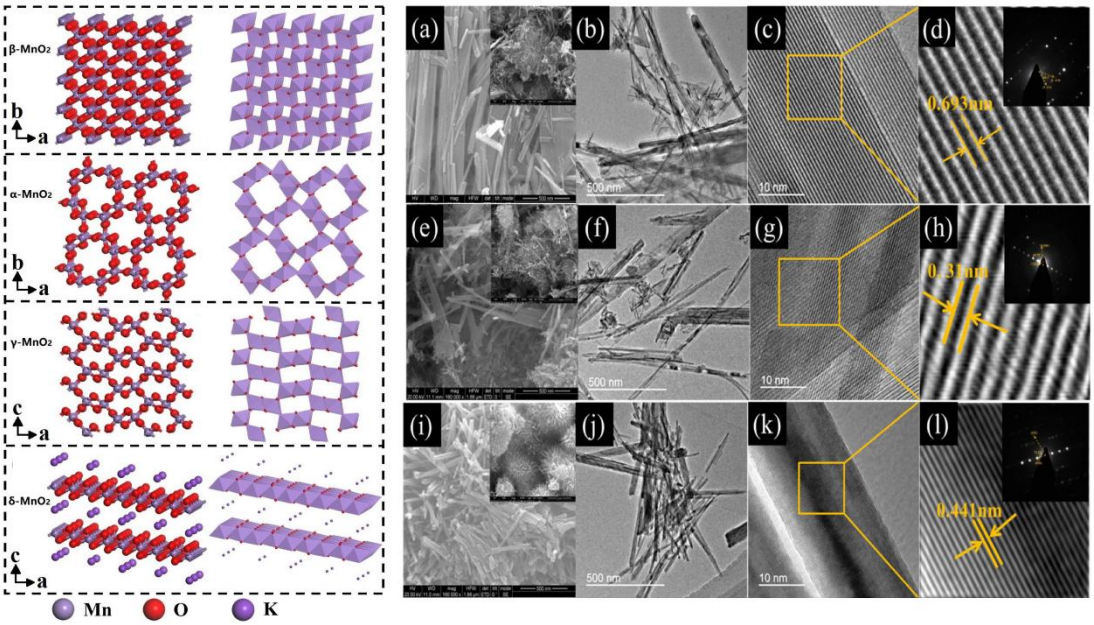

Figure 2. Crystal structure of β-, α-, γ-, and δ-MnO_2 [23]. SEM and TEM images of α-MnO_2-110 (**a**–**d**), α-MnO_2-310 (**e**–**h**), and α-MnO_2-210 (**i**–**l**) [24]. Copyright 2019 and 2021, Elsevier B.V.

3.1.2. Cerium Oxides

Ce has great oxygen storage capacity, abundant acidic sites, and unique valence change capability (Ce^{4+} to Ce^{3+}), which makes the CeO_2 materials rich in defects and oxygen vacancies in the crystal, thus giving CeO_2 excellent redox properties in the catalytic combustion of toluene [40,41]. However, due to the limitation of its own structure and physicochemical properties, a pure CeO_2 catalyst can only enable the complete oxidation of toluene in the high-temperature region. Therefore, enhancing the low-temperature performance of CeO_2 catalysts has been widely reported in the literature (Table 1).

Hu et al. [29] synthesized CeO_2 microspheres with layered structures self-assembled by nanowires using a hydrothermally driven assembly method. The catalytic activity of the novel layered CeO_2 catalysts was significantly better than that of the similar non-porous catalysts prepared by the conventional hydrothermal method. Compared with the bulk cerium dioxide, the nanowire self-assembled layered CeO_2 exhibited better combustion activity at low temperatures, with toluene conversion of more than 90% even at 210 °C. The high catalytic activity could be due to the large surface area and the layered porous structure, which contributed to the exposure of more surface oxygen vacancies. Feng et al. [30] prepared CeO_2 catalysts in rod, hollow spherical, and cubic forms via hydrothermal methods. The results indicated that CeO_2 hollow spheres exhibited the best catalytic activity for the degradation of toluene. This was because CeO_2 hollow sphere catalysts have the largest specific surface area and the most oxygen vacancies. Mi et al. [31] prepared CeO_2 catalysts with different morphologies (nanopolyhedra, nanorods, and nanocubes) using a hydrothermal method. CeO_2 nanopolyhedra have better catalytic activity than CeO_2 nanorods and nanocubes. The results demonstrated that CeO_2 with distinctive morphologies has different oxygen distributions, especially the surface lattice oxygen distribution. The surface lattice oxygen concentration showed a linear relationship with the catalytic activity, indicating that the surface lattice oxygen participated in the oxidation process of toluene. Yan et al. [32] prepared CeO_2 materials with nanotube, nanobelt, and wire-in-nanotube morphologies using the electrostatic spinning technique. The high catalytic activity of CeO_2-nanobelt catalysts could be attributed to their porous nanoribbon morphology, large specific surface area, and abundant surface oxygen vacancies. Chen et al. [33] successfully prepared CeO_2 catalysts with mesoporous structures by the in situ pyrolysis of Ce-MOF precursors. In comparison with commercial and co-precipitation-

prepared CeO_2 catalysts, CeO_2-MOF/350 catalysts exhibited a stronger ability to achieve 100% conversion, whereas CeO_2-C and CeO_2-P catalysts usually require higher temperature regions to complete the oxidation of toluene. This high catalytic activity could be attributed to the large specific surface area, rich three-dimensional pore channels, small average grain size, higher reactive oxygen species and oxygen vacancy concentrations, higher relative percentages of Ce^{3+}/Ce^{4+} and O_{Sur}/O_{Latt}, better low-temperature reducibility, and more acidic sites. In conclusion, the main method for improving the performance of CeO_2-catalyzed toluene degradation is to promote the adsorption and activation of molecular oxygen through the formation of oxygen vacancies, thus further improving the oxygen storage and release capacity of CeO_2 catalysts. In this process, surface vacancies tend to adsorb and activate gaseous O_2 to form adsorbed oxygen species, while bulk vacancies increase the activity and mobility of lattice oxygen species through transport effects [42]. Adsorbed oxygen is mainly involved in the chemisorption and partial oxidation of toluene. As the temperature increases, the lattice oxygen of the catalyst promotes the decomposition of the aromatic ring, which further accelerates the conversion of intermediates to CO_2 and H_2O.

3.1.3. Cobalt Oxides

Co_3O_4, a typical spinel metal oxide, has received wide attention in the catalytic combustion of VOCs. It is considered as one of the most active inexpensive metal catalysts, and the high activity is mainly related to the mobile oxygen species and high oxygen-binding rate in its spinel structure [41,43]. The catalyst has high reduction, more oxygen vacancies, and a high concentration of electrophilic oxides. The catalytic activity of the Co_3O_4 catalyst depends mainly on the microscopic morphology, preparation method, processing conditions, oxidation state, and surface area, and the Co_3O_4 catalyst is the most efficient catalyst for the complete oxidation of toluene. Therefore, efforts have been devoted to the development of Co_3O_4-based catalysts with various structures and morphologies (Table 1).

Ren et al. [34] reported a series of 1D-Co_3O_4, 2D-Co_3O_4, and 3D-Co_3O_4 materials and investigated their applications in the catalytic combustion of toluene. The results showed that 3D-Co_3O_4 had the best activity with 90% conversion of toluene at about 238 °C. This can be attributed to the excellent properties of 3D-Co_3O_4 nanoflowers with low reduction temperature, large specific surface area, abundant surface reactive oxygen species, and rich defect structure. The successful synthesis of 3D Co_3O_4 nanocatalysts by a hydrothermal method can also result in different morphologies, including 3D hierarchical flake-stacked fan-shaped Co_3O_4 (S), 3D hierarchical needle-stacked begonia-like Co_3O_4 doublets (N), 3D hierarchical flat-stacked Co_3O_4 flowers (P), and 3D hierarchical cubic-stacked Co_3O_4 microspheres (C) [35]. As confirmed by HRTEM analysis, they mainly had exposed (112), (110), (110), and (111) crystal faces, respectively. The catalytic activity for toluene oxidation decreased as follows: C > P > N > S. However, in the 3D hierarchical Co_3O_4 catalysts with distinct different morphologies and exposed crystal faces synthesized by Liu et al. [44], the S-160 catalyst with exposed (110) crystal faces had a higher oxidation activity with toluene conversion up to 50% at 234 °C, which was 17 °C lower than the material with predominantly exposed (111) faces. This was mainly due to its abundant adsorbed oxygen, good redox properties, and highly defective structure.

A metal–organic framework (MOF) is a kind of hybrid material with a high specific surface area, high porosity, and tunable structure formed by an organic ligand and a metal ion through coordination bond assembly [45]. Templating is a commonly used method for preparing nanomaterials and allows the structure and morphology of the material to be designed according to the requirements. MOFs have received much attention as novel precursors for the synthesis of porous inorganic materials. Among them, zeolitic imidazolate frameworks (ZIFs) are a subfamily of metal–organic frameworks (MOFs) composed of Zn^{2+} or Co^{2+} and imidazole or imidazole derivatives; they combine the high stability of inorganic zeolites with the high porosity of MOFs [38]. The versatility of Co-

ZIFs and the low cost and simple synthesis methods make them the preferred precursors for Co_3O_4 [46]. It is known that in the spinel structure of Co_3O_4, Co^{3+} is usually present in octahedral coordination, while Co^{2+} is present in tetrahedral coordination [47]. Co^{3+} is usually regarded as the active site for VOC combustion, as evidenced by previous studies [37,48].

Han et al. [36] accurately regulated the growth of ZIF structures by varying the distribution of N elements on the nanofiber surface. The N-element microenvironment on the nanofiber surface affects not only the growth mechanism of ZIFs, but also the molecular space configuration (tetrahedral and octahedral structures of Co_3O_4). In order to expose more Co^{3+}, further octahedral structure formation was induced by using the triethylamine (TEA) induction method. The results demonstrated that the prepared Co_3O_4 materials possessed more Co^{3+} and exhibited the best catalytic performance (90% catalytic efficiency at 220 °C). Zhao et al. [37] successfully synthesized a series of Co_3O_4 hollow polymorphs with different sizes by the pyrolysis of ZIF-67. The samples still maintained the nanosize and shape of the MOF precursors. The Co_3O_4-400 catalyst with a particle size of 400 nm showed good catalytic performance with a complete conversion temperature of 280 °C for toluene (T_{100}). Co_3O_4 catalysts prepared with distinct shapes and ligands of Co-MOF as precursors also exhibited different physicochemical properties [38]. A series of mesoporous Co_3O_4 samples prepared by pyrolysis of dodecahedral ZIF-67, rod-shaped MOF-74, and octahedral ZSA-1 exhibited toluene catalytic activity in the following sequence: ZSA-1-Co_3O_4 (octahedral-shaped N-O-ligand) > MOF-74-Co_3O_4 (rod-shaped N-O-ligand) > ZIF-67-Co_3O_4 (dodecahedral-shaped N-O-ligand). This could be attributed to the differences in different exposure surfaces, low-temperature reducibility, specific surface area, and ratio of Co^{3+}/Co^{2+} and O_{ads}/O_{latt}.

3.2. Multi-Oxide Composites

The poor chemical and thermal stability of single metal oxides usually leads to particle aggregation and ultimately to a decrease in catalytic performance [49]. Multiple transition metal oxide composites can further contribute to thermodynamic stability and modulate the electronic structure and surface properties compared to single metal oxides [46,50–70]. Multi-oxide composites, such as MnO_x doped, loaded, or forming solid solutions with other transition metals, can exhibit altered physicochemical properties and create synergistic effects in the VOC conversion process [21]. This synergistic property may lead to better surface mobility of reactive oxygen species and promote the electron transport between toluene and the material, thus enhancing the reaction between toluene and reactive oxygen species. Therefore, multi-oxide composites are of interest. The toluene catalytic degradation performance and reaction conditions of the binary composites are summarized in Table 2. The results indicate that different transition metal oxide blends also exhibit different toluene catalytic behaviors under the synergistic effect.

Table 2. Catalytic activity for toluene combustion over the binary composites reported in the recent literature.

Catalyst	Synthesis Method	Toluene Conc.	WHSV or GHSV ($mL \cdot g^{-1} \cdot h^{-1}$ or h^{-1})	Activity T_{90} (°C)	Ref.
1Cu1Mn	MOF template	1000 ppm	60,000 $mL \cdot g^{-1} \cdot h^{-1}$	208	[50]
CuO-MnO_x-500	Sol–gel	600 ppm	19,800 $mL \cdot g^{-1} \cdot h^{-1}$	228	[51]
$CuMnO_x$-HS	Oxidation method	500 ppm	60,000 $mL \cdot g^{-1} \cdot h^{-1}$	212	[52]
CuO/MnO_2-R-10	Solid-state redox strategy	500 ppm	60,000 $mL \cdot g^{-1} \cdot h^{-1}$	234	[53]
$MnCu_{0.5}$	Hydrothermal–redox	1000 ppm	20,000 $mL \cdot g^{-1} \cdot h^{-1}$	210	[54]

Table 2. *Cont.*

Catalyst	Synthesis Method	Toluene Conc.	WHSV or GHSV ($mL \cdot g^{-1} \cdot h^{-1}$ or h^{-1})	Activity T_{90} (°C)	Ref.
Tunneled Cu-Mn	Hydrothermal method	1000 ppm	10,000 h^{-1}	169	[55]
L-to-T Cu-Mn				199	
Layered Cu-Mn				221	
$Mn_{0.6}Ce_{0.4}O_2$	Redox–precipitation and hydrothermal	500 ppm	22,500 h^{-1}	207	[56]
Ce-Mn-O_x	Hydrothermal method	500 ppm	60,000 h^{-1}	246	[57]
	Citrate sol–gel			249	
	Co-precipitation			259	
	Impregnation			261	
$Mn_{0.85}Ce_{0.15}$	Co-precipitation and hydrothermal	1000 ppm	32,000 $mL \cdot g^{-1} \cdot h^{-1}$	216	[58]
$Mn_{12}Ce_1$-SW	SPT process	1000 ppm	15,000 $mL \cdot g^{-1} \cdot h^{-1}$	277	[59]
$CoMn_2O_4$	Sol–gel	500 ppm	22,500 $mL \cdot g^{-1} \cdot h^{-1}$	210	[60]
Nanocrystal-like Mn_1Co_2	Hydrothermal method	1000 ppm	30,000 $mL \cdot g^{-1} \cdot h^{-1}$	240	[61]
Co_3O_4/α-MnO_2	Solvothermal method	500 ppm	60,000 h^{-1}	248	[62]
MnO_2@ Co_3O_4	ZIF-derived Co_3O_4 template	1000 ppm	48,000 $mL \cdot g^{-1} \cdot h^{-1}$	229	[63]
Ni-MnO_2	EG reduction strategy	1000 ppm	20,000 $mL \cdot g^{-1} \cdot h^{-1}$	199	[64]
Cu-MnO_2				217	
Co-MnO_2				218	
$Mn_{0.3}Zr_{0.7}O_2$	Impregnation	1000 ppm	60,000 $mL \cdot g^{-1} \cdot h^{-1}$	235	[65]
MnO_x@ZrO_2-NA	MOF template	1000 ppm	60,000 $mL \cdot g^{-1} \cdot h^{-1}$	260	[66]
CeCu-HT	Hard template	10,000 ppm	66,000 $mL \cdot g^{-1} \cdot h^{-1}$	225	[67]
CeCu-CA	Complex method			270	
Cu_1Ce_3	Co-precipitation	1000 ppm	30,000 h^{-1}	180	[68]
Ce_1Co_2	Carbon xerogel template	1000 ppm	60,000 h^{-1}	241	[69]
$Co_{0.2}Ce_{0.8}O_2$-δ	Hydrothermal	1000 ppm	20,000 $mL \cdot g^{-1} \cdot h^{-1}$	230	[70]
$Co_1Cu_1O_x$	Co-MOF template	1000 ppm	20,000 $mL \cdot g^{-1} \cdot h^{-1}$	208	[46]
$Co_1Mn_1O_x$				227	
Co_3O_4				239	
$Co_1Fe_1O_x$				234	
$Co_1Ni_1O_x$				246	

3.2.1. Binary Composites

The integration of MnO_x with other metal oxides such as CuO, CeO_2, Co_3O_4, NiO, and ZrO_2 is an effective strategy for improving catalytic performance. The introduction of secondary metals can effectively reduce the crystallinity of MnO_x and produce intermetallic synergistic effects, which can introduce a large number of oxygen vacancies and improve the catalytic activity. The potential of $CuMnO_x$ oxides for the oxidation reaction of VOCs is well known in industry [41]. For instance, the 1Cu1Mn reported by Hu et al. [50] exhibited great toluene oxidation performance and corrosion resistance. The experimental results indicated that the catalytic activity of both binary composites for toluene was higher than that of single MnO_x and CuO_x. During the preparation of the materials, the

toluene conversion first increased and then decreased with the annealing temperature increasing, and the best toluene oxidation activity was acquired for the catalyst annealed at 500 °C [51]. Liu et al. [52] prepared hollow spherical $CuMnO_x$-HS catalysts by an oxidation method using Cu_2O as a template; this special oxidation method enhanced the synergistic interaction between Mn and Cu, which resulted in $CuMnO_x$-HS with large specific surface area, good reduction, oxygen mobility, and rich adsorbed oxygen species, thus promoting the catalytic efficiency of toluene oxidation. Liu et al. [53] modified the surface defect concentration of α-MnO_2 using a solid-state redox strategy. Surface reduction of α-MnO_2 by Cu_2O greatly improved the oxygen vacancy concentration for CuO/MnO_2-R catalysts. The T_{90} of Cu_2O-reduced CuO/MnO_2-R-10 catalysts with increased structural defects was 36 and 32 °C lower than that of the α-MnO_2 and CuO-reduced CuO/MnO_2-10 catalysts, respectively. The lattice defects and oxygen vacancy concentration of the prepared catalysts can also be regulated by controlling the Mn/Cu molar ratio. Spinel Mn-Cu oxides synthesized by hydrothermal–redox method with Mn/Cu molar ratios of 2/1 had abundant adsorbed oxygen, high Cu^+ and Mn^{3+} contents, and good low-temperature reduction. They exhibited the highest catalytic activity, excellent durability, and water resistance in the total oxidation of toluene [54]. In addition, Luo et al. [55] designed a series of Cu-modified MnO catalysts with tunneling, layered, and transition structures using a hydrothermal method. The tunnel structure catalysts showed the best performance and excellent water resistance among the three Mn-Cu oxides. This could be attributed to the catalyst having abundant oxygen species, good low-temperature reducibility, a lower average Mn oxidation state, and a large specific surface area.

CeO_2 has attracted attention for its abundant oxygen defects and high oxygen storage ability for rapid reversible redox cycling (Ce^{4+}/Ce^{3+}). The doping of Ce into Mn-based catalysts could form abundant Ce^{3+} and Mn^{3+}, which facilitates the generation of oxygen vacancies and enhances the migration of active oxygen in the catalyst. The synthesized Mn-Ce mixed oxides can outperform the single metal oxides in the oxidation of toluene [56]. Zhang et al. [57] prepared Ce-Mn-O_x catalysts using four methods: co-precipitation (CP), hydrothermal (HT), impregnation (IM), and citrate sol–gel (SG). CM-HT prepared by HT methods had more crystallization defects, oxygen vacancies, and surface adsorbed oxygen and a normalized conversion rate, thus showing the best catalytic oxidation performance for toluene. Liao et al. [58] successfully synthesized Mn-Ce nanorod materials with different Mn contents, which will affect the catalytic activity and result in higher stability. The right ratio of Mn and Ce oxides could induce the formation of a solid solution in catalysts and more Mn^{4+} and oxygen vacancies, which were key to maintaining high activity and stability. Li et al. [59] found that trace CeO_2-doped δ-MnO_2 catalysts with a high Mn^{4+}/Mn^{3+} ratio, at lower reduction temperatures, could convert toluene with an efficiency of 90% at 277 °C. The incredible oxidation activity of the $Mn_{12}Ce_1O_x$ catalyst might be due to the synergistic interaction of highly dispersed CeO_2 nanoparticles with the δ-MnO_2 substrate at the interface.

Researchers also found that Mn-Co spinel catalysts have high catalytic performance and stability in catalytic oxidation. In the spinel (AB_2O_4) structure, A and B sites are in tetrahedral and octahedral positions, respectively. Adjacent cations (A and B) can optimize catalytic performance through electron transfer. Dong et al. [60] studied the catalytic oxidation of toluene by nanoflower-shaped $CoMn_2O_4$ synthesized by the sol–gel method. The results indicated that the activation energy (35.5 kJ/mol) for toluene oxidation catalyzed by spinel-type $CoMn_2O_4$ was lower than that of using metal oxides (Co_3O_4, MnO_x, and Co_3O_4/MnO_x). Among the numerous Mn-Co solid solutions, strong interactions were formed between MnO_x and CoO_x, which promoted the toluene oxidation activity. At a Mn/Co molar ratio of 1:2, the Mn-Co material prepared by a two-step hydrothermal method could achieve complete conversion of toluene at 250 °C [61]. The unique high porosity, large surface area, and high concentration of reducible oxygen are the main reasons for the significantly enhanced catalytic activity of these spinel binary materials. The construction of heterogeneous structures by interfacial engineering is another effective

way to improve catalytic performance. Liu et al. [62] successfully immobilized Co_3O_4 on the surface of different phases of MnO_2 and investigated the effect of different interfaces of Co_3O_4-MnO_2 for the catalytic oxidation of toluene. The temperature order of T_{90} was as follows: Co_3O_4/α-MnO_2 (248 °C) < Co_3O_4/γ-MnO_2 (266 °C) < α-MnO_2 (270 °C) < γ-MnO_2 (280 °C) < Co_3O_4/β-MnO_2 (282 °C) < β-MnO_2 (288 °C). Ren et al. [63] successfully grew ZIF-derived Co_3O_4 in situ on a one-dimensional α-MnO_2 material (α-MnO_2@Co_3O_4). The synthesized α-MnO_2@Co_3O_4 catalysts exhibited excellent catalytic performance at about 229 °C (T_{90}), which was 47 and 28 °C lower than that of pure α-MnO_2 nanowires and Co_3O_4-b, respectively. The interfacial effect resulting from the coupling between α-MnO_2 and Co_3O_4 was the main reason for the enhanced activity of these catalysts. The construction of the Co_3O_4-MnO_2 interface significantly increased the vacancy concentration, accelerated lattice oxygen mobility, improved the redox cycle of Mn^{4+}/Mn^{3+} and Co^{2+}/Co^{3+}, and greatly enhanced the catalytic toluene oxidation.

The interaction of Mn and Ni with Zr ions can likewise enhance the redox ability of Mn-based binary catalysts. Importantly, promoting the uptake and activation of molecular oxygen at defective sites can significantly improve the oxidation activity of the catalyst. Dong et al. [64] synthesized a series of Ni-, Cu-, and Co-doped α-MnO_2 catalysts (M-MnO_2) for the catalytic oxidation of toluene using the reduction of $KMnO_4$ by ethylene glycol (EG) for the first time. Significant low-temperature activity (T_{90} = 199 °C) was obtained over Ni-MnO_2 catalysts. This could be attributed to the Ni^{2+} substitution doping into the octahedral MnO_6 backbone which improved the formation of active lattice oxygen and active oxygen mobility. Yang et al. [65] prepared oxygen vacancy-containing $Mn_xZr_{1-x}O_2$ catalysts by partial substitution of Zr^{4+} for low-valent manganese (Mn^{2+}). Their performance with better toluene conversion and specific reaction rate could be due to the increase in oxygen vacancy concentration. Li et al. [66] proposed a double-constrained strategy to reduce the agglomeration of Mn and prepared well-dispersed MnOx@ZrO_2 catalysts using metal–organic frameworks. With a grain size of 17.65 nm, both Mn and Zr elements were uniformly dispersed, obtaining higher toluene oxidation efficiency than MnO_x.

Binary mixtures of Ce, Co, and Cu formed with each other are also common catalysts for toluene oxidation. By compounding, the catalytic performance can be substantially increased. Zhou et al. [67] prepared Ce-Cu composite oxides using the complex method (CeCu-CA) and hard template method (CeCu-HT). The results showed that the catalytic activity of the CeCu-HT catalyst was higher than that of CeCu-CA in air, which could be attributed to the difference in composition and structure. Song et al. [68] reported a series of Cu-Ce binary oxides for the catalytic oxidation of toluene using the co-precipitation method. The Cu_1Ce_3 catalysts exhibited superior toluene oxidation activity due to higher specific surface area, better low-temperature reduction, and stronger Cu-Ce synergy. Carabineiro et al. [69] synthesized binary oxides of Ce-Co and La-Co using an external template method and evaporation. The mixed oxides were superior in toluene oxidation compared to single oxides, and the Ce-Co binary oxides were more active than the La-Co catalyst. The results indicated that the strong interaction between Ce/La and Co led to a sufficient dispersion in the binary system, which improved the specific surface area and reduction of the catalyst. Ismail et al. [70] prepared a series of $Co_xCe_{1-x}O_2$-δ (x = 0.05 ~ 0.6) oxides using a hydrothermal method, and the $Co_xCe_{1-x}O_2$-δ had higher catalytic activity than pure Co_3O_4 and CeO_2. This good performance was mainly due to the strong interaction between Ce and Co in a solid solution resulting in an abundance of surface reactive oxygen species and an increase in surface Co^{3+} and Ce^{3+} species. For $Co_1Y_1O_x$ (Y = Cu, Mn, Fe, Ni) catalysts, the introduction of different dopants had a significant effect on the physicochemical properties of the catalysts, but the best catalytic activity was obtained for $Co_1Cu_1O_x$ [46]. It was due to the improved catalytic properties of $Co_1Cu_1O_x$ with larger specific surface area, smaller grain size, more surface defect sites, higher Co^{3+} and O_{ads}, and better reduction. Xu et al. [71] prepared bimetallic CuO/Co_3O_4 oxides by in situ pyrolysis using the MOF template method for partially replacing the Cu ions with Co ions. Compared with CuO, Co_3O_4, and Mix-CuO/Co_3O_4, CuO/Co_3O_4 had the best catalytic activity, accomplishing

90% conversion efficiency at 229 ◦C. This could be attributed in general to the lower temperature reducibility, high degree of dispersion of CuO/Co_3O_4, more reactive oxygen species, abundant lattice defects, and higher molar ratios of Co^{3+}/Co^{2+} and O_{latt}/O_{ads}.

3.2.2. Perovskite Oxides

Perovskite oxides (ABO_3) have become a common choice for catalysts of aromatic VOCs due to their special structure and properties [72]. In the ABO_3 chemical formula, A is a large cation with 12 times the coordination number (A-site) and B is a small cation with 6 times the coordination number (B-site), coordinated to the oxygen anion [10]. Perovskite catalysts are characterized by good thermal stability due to high-temperature calcination conditions, the unique valence of transition metal ions, easy-to-adjust redox performance, and good low-temperature reduction performance [10,72]. Currently, Mn-based perovskites are the most common catalysts [39]. The Mn site in the structure can provide more oxidation states, and the rare earth elements at the A site have strong oxygen storage capacity, which can promote the generation of active oxygen in the reaction. For example, Zhang et al. [73] synthesized $LaMnO_3$ perovskite oxides using three methods: citric acid sol–gel (SG), co-precipitation (CP), and glycine combustion (GC). The high specific surface area, the concentration of adsorbed oxygen species, and the low reduction temperature on the surface were in the order of LMO-SG > LMO-CP > LMO-GC, which matched well with the order of catalytic performance. Liu et al. [74] synthesized highly reactive $SmMnO_3$ oxides by self-fusion polymerization, co-precipitation, impregnation, and sol–gel methods. The $SmMnO_3$ prepared by self-fusion polymerization had the highest catalytic performance. This was associated with its higher lattice oxygen content, optimal low-temperature reduction, and higher surface Mn^{4+}/Mn^{3+} ratio. In addition, Chen et al. [75] successfully prepared multi-shell spherical $PrMnO_3$ oxides for the first time and applied them to the catalytic combustion of CO and toluene. Compared with the catalysts prepared by the conventional co-precipitation method ($PrMnO_3$-CP), $PrMnO_3$-HoMSs showed higher catalytic activity for the oxidation of both CO and toluene. The high Mn^{4+}/Mn^{3+} molar ratio, the improved low-temperature reduction, and the increased reactive oxygen species were the main reasons for the good catalytic performance of $PrMnO_3$-HoMSs.

The catalytic performance of perovskite oxides depends mainly on the nature of the A and B elements and their valence states, and the A-site ions are usually considered to be catalytically inactive. Therefore, the catalytic performance of perovskite is usually limited by its small surface area and the relatively small amount of surface B-site cations that participate in the catalytic oxidation of aromatic VOCs. To improve the redox performance of perovskite, perovskite oxides are often loaded on carriers such as Al_2O_3, CeO_2, zeolite, and cordierite [10,76]. Among various carriers, CeO_2 is one of the most popular carriers due to its high oxygen storage capacity with abundant oxygen vacancy properties. Wang et al. [76] prepared different morphologies of CeO_2 carriers (rods, cubes, and polyhedra) using a hydrothermal method. The $La_{0.8}Ce_{0.2}MnO_3/CeO_2$ nanopolyhedra exhibited catalytic properties such as small particle size, high specific surface area, more oxygen vacancies, and active oxygen species. Moreover, the establishment of $LaMnO_3/MnO_2$ interface is beneficial for acquiring a great catalytic capacity for toluene oxidation, while the conventional solid-phase and sol–gel methods have problems in regulating the formation of $LaMnO_3$ and immobilizing $LaMnO_3$ on a specific crystalline phase, δ-MnO_2. Yang et al. [77] first assembled $LaMnO_3$ on δ-MnO_2 using a simple gunpowder-like combustion method. Compared with the conventional solid-state method and sol–gel method, the catalyst synthesized by this strategy can achieve complete oxidation of toluene at 275 °C. This was because the interaction between $LaMnO_3$ and δ-MnO_2 improved the redox ability. Moreover, a typical strategy for enhancing the catalytic activity of perovskite is the loading of MO_x (metal oxides) on ABO_3, where perovskite can be used not only as an active component but also as a carrier. Suárez-Vázquez et al. [78] focused on the effect of B-site cations in the dendritic $SrTiO_3$ perovskite on the toluene catalytic behavior. Unlike the role of Cu on the catalyst surface, the addition of Mn leads to Mn^{4+} binding at the Ti^{4+} site in

the perovskite structure. This interaction resulted in the highest catalytic performance of the Mn-doped catalyst for the complete conversion of toluene to CO_2 at less than 350 °C.

3.2.3. Multiple Composites

Multiple composites are multi-element complex oxides composed of three or more transition metal oxides. The tight mixing of these components in the multiple composites can further enhance the interaction and thus the catalytic activity. Clarifying the role of each element and the interactions between these composites is beneficial for designing catalysts for applications under actual working conditions. Dula et al. [79] prepared layer-doped $MgMnAlNO_3$ and interlayer-doped $MgAlMnO_4$ by co-precipitation and anionic precipitation, respectively. The $MgMnAlNO_3$ had higher Mn^{4+} phase reduction compared to $MgAlMnO_4$, which was considered to be the main reason for the higher oxidation performance of the sample in the total oxidation of toluene. Lu et al. [80] prepared Cu-Mn, Cu-Ce, and Cu-Mn-Ce mixed oxides by the sol–gel method. The Cu-Mn-Ce ternary oxide showed the highest catalytic activity. The Cu and Mn atoms were doped into the CeO_2 lattice to form a cerium-based solid solution, which resulted in better interactions of Cu-Mn-Ce, which enhanced the catalyst reduction and oxygen mobility. Hu et al. [81] synthesized a series of spongy Cu-Mn-Ce ternary oxides by a surfactant-modified co-precipitation method, and the catalytic performance was optimized at the mixing ratio of 1:5:5. The results indicated that the appropriate amount of Cu facilitated the combination of highly reducing Mn^{4+} with Ce lattice to form a $MnCeO_x$ solid solution, which improved the redox behavior and produced a large amount of active oxygen at the $CuO_x/MnCeO_x$ interface, thus facilitating the combustion of toluene at lower temperatures. Wang et al. [82] doped Cu into Co-Ga layered spinel catalysts using layered double hydroxides as precursors. The difference in the radii of Cu(II) and Co(II) ions resulted in lattice distortion and increased surface oxygen defects, adsorbed oxygen species, and reducibility. This greatly enhanced the catalytic efficiency of toluene oxidation. In conclusion, the results of all the above studies demonstrate the importance of Cu in the preparation of multiplex composite catalysts. Wang et al. [83] synthesized $Cu_xCe_{1-x}Fe_2O_4$ (x = 0, 0.2, 0.5, 0.8, 1) catalysts using the sol–gel method. The suitable Ce ratio doped $Cu_{0.8}Ce_{0.2}Fe_2O_4$ showed the highest oxidation performance for toluene. The excessive increase in Ce doping leads to the gradual loss of $CuFe_2O_4$ spinel structure, and the catalytic combustion activity is significantly suppressed. Therefore, it can be assumed that suitable Ce doping into $CuFe_2O_4$ can increase its oxygen storage capacity and enhance the catalytic activity of toluene oxidation. Liu et al. [84] grew γ-MnO_2 in situ on $SmMnO_3$ perovskite prepared by a one-step roasting strategy. The prepared γ-$MnO_2/SmMnO_3$ showed better performance in the catalytic activity of aromatic VOCs in wet air compared to $SmMnO_3$ and γ-MnO_2. This might be due to its higher surface molar ratio of O_{latt}/O_{ads} and better reducibility at low-temperature.

3.3. Supported Metal Oxide Catalysts

A supported metal oxide catalyst is a catalyst whose active components and cocatalysts are uniformly dispersed and loaded on a specially selected carrier. The selection of a suitable carrier can provide reaction space for the catalytic reaction [21]. A catalyst carrier with a high specific surface area and porous characteristics can improve the mass transfer efficiency and adsorption capacity of toluene. In addition, the degradation behavior is closely related to the nature of the carrier. Some high-acidity carriers can also directly participate in the catalytic reaction and contribute to better activity and selectivity. In addition, the strong active phase–carrier interaction effect in the supported metal catalysts has a significant positive impact on their catalytic performance. As shown in Table 3, the common conventional carriers are TiO_2 [85,86], Al_2O_3 [87–92], ZSM-5 [93,94], HZSM-5 [95], beta (BEA) zeolite [96], clinoptilolite-type zeolite [97], MCM-41 [98], cordierite [99] and pillared clay [100,101].

Table 3. Catalytic activity for toluene combustion over supported metal oxide catalysts reported in the recent literature.

Catalyst	Synthesis Method	Toluene Conc. (ppm)	WHSV or GHSV ($mL \cdot g^{-1} \cdot h^{-1}$ or h^{-1})	Activity T_{90} (°C)	Ref.
$9.5MnO_2/\alpha$-Al_2O_3	Impregnation	1000	15,000 h^{-1}	289	[87]
$Cu_{0.5}Mn_{0.75}/\alpha$-Al_2O_3	Impregnation	1000	120,000 h^{-1}	332	[88]
$CuMn_{(y)}O_x/\gamma$-Al_2O_3	Impregnation	1200	15,000 h^{-1}	229	[89]
CuO/Al_2O_3	Impregnation	1000	200,000 $mL \cdot g^{-1} \cdot h^{-1}$	320	[90]
CuV/ZSM-5	Hydrothermal method	800	15,000 h^{-1}	315	[93]
10%MnOx/HZSM-5	Impregnation	1000	15,000 $mL \cdot g^{-1} \cdot h^{-1}$	261	[95]
$9.5MnO_2$/clinoptilolite-type zeolite	Impregnation	1000	15,000 h−1	297	[97]
Fe-Ti-PILC	Impregnation	1000	60,000 $mL \cdot g^{-1} \cdot h^{-1}$	347	[100]
10%Co-5%Ce/SPC	Soft template	1000	20,000 h^{-1}	175	[101]
10%Co-5%Ce/MMT				208	

Different carrier materials have a crucial influence on catalytic performance. Pozan et al. [87] compared the effects of a series of carriers loaded with MnO_2 components (α-Al_2O_3 and γ-Al_2O_3 obtained from boehmite, commercial γ-Al_2O_3, SiO_2, TiO_2, and ZrO_2) on the toluene degradation efficiency. Among them, the $9.5MnO_2/\alpha$-Al_2O_3(B) catalyst had the highest catalytic performance with 90% toluene conversion at 289 °C. Wang et al. [88] synthesized Cu/Mn-loaded γ-Al_2O_3 catalysts by the impregnation method. The results indicated that CuO and MnO could be highly dispersed on the γ-Al_2O_3 carrier. In practical applications, it was found that the activity of catalytic oxidation of VOCs is negatively affected by the water vapor of the feed material. However, catalysts with different carriers can weaken the inhibition of water vapor. For the catalysts loaded with CuMn, the water durability followed the order $CuMn_{(1)}O_x$/cordierite > $CuMn_{(1)}O_x/TiO_2$ > $CuMn_{(1)}O_x/\gamma$-Al_2O_3 [89]. In addition, the catalytic performance largely depended on the reducibility of the active component. The catalytic performance of reducible materials is usually much higher than that of irreducible materials [90]. Under the same metal oxide load (10 wt% M_xO_y/Al_2O_3), CuO/Al_2O_3 was by far the most active catalyst in the series, followed by catalysts loaded with MnO, V_2O_5, Cr_2O_3, and CeO_2, and finally, Al_2O_3-loaded MgO, Nd_2O_3, CsO, and ZrO_2 catalysts were practically inactive [90]. Saqer et al. [92] used the impregnation method to load Cu-Mn, Mn-Ce, and Cu-Ce on Al_2O_3 for the catalytic oxidation of toluene. The results demonstrated that the catalytic activity of mixed metal oxides was also significantly improved by optimizing the M_xO_y loading and the composition of the multi-metal oxides.

Zeolite is an excellent carrier of transition metal oxides because of its unique porous structure, thermal stability, acid resistance, and catalytic properties. Its catalytic properties are determined by the acidic distribution, pore size, and cation exchange properties. Different experimental conditions for the preparation of supported transition metals affect this catalytic property. Palacio et al. [93] deposited copper vanadate precursors on two types of carriers, ZSM-5 and amorphous SiO_2, by a hydrothermal method and a mechanical mixing method, respectively. The CuV_2O_6 deposited on ZSM-5 using the hydrothermal method showed the best oxidation efficiency. This might be related to the smaller particle size and higher dispersion of the active component on the carrier. Zhang et al. [95] synthesized a series of 10% MnO_x/HZSM-5 catalysts with different ratios of Si/Al (Si/Al = 25, 50, and 75) using the primary impregnation method. The results showed that all samples

had similar structures and redox properties but differed in surface acidity. The catalytic activities of these catalysts were 10%MnO_x/HZSM-5-25 > 10% MnO_x/HZSM-5-50 > 10% MnO_x/HZSM-5-75 in descending order. The 10%MnO_x/HZSM-5-25 had excellent catalytic stability under dry conditions and high water resistance under wet conditions. In particular, beta (BEA) zeolite is an industrially produced high-silica zeolite with a 3D structure and three perpendicular 12-ring channel systems [96]. The pore size is generally larger than that of ZSM-5. The activity of MnO_2-loaded BEA zeolite catalysts was significantly higher than that of unloaded and MnO_2-loaded ZSM-5 [96].

Natural clay minerals have received great attention owing to their low price, environmental compatibility, high selectivity, and plasticity [100,101]. Montmorillonite (MMT) is a class of clay minerals with a special layered structure. In general, pillared montmorillonite catalysts (PILC) are synthesized by ion exchange (TiO_2, SiO_2, etc.) of Na^+ and Ca^{2+} adsorbed in the montmorillonite layer with organic or inorganic ions [102]. Compared with montmorillonite, PILC has the advantages of large specific surface area, uniform pore size distribution, and good thermal stability, creating quality conditions as catalyst carriers. Liang et al. [100] synthesized Ti-pillared montmorillonite (Ti-PILC) catalysts loaded with Fe and used them successfully for the catalytic oxidation of toluene. Cheng et al. [101] prepared mesoporous Si-pillared montmorillonite (SPC) using a soft template strategy. Compared with the original montmorillonite, the thermal stability was improved, the specific surface area increased from 30 to 453 m^2/g, and the layer spacing of SPC increased from 0.96 nm to 2.61 nm. SPC nanocatalysts loaded with Co_3O_4 and rare earth (Y, La, Ce, Pr, and Nd) were synthesized using the deposition–precipitation strategy. Among them, 10%Co-5%Ce/SPC had the highest performance and achieved 98% conversion for catalytic combustion of toluene at 200 °C.

4. Oxidation Kinetics and Catalytic Mechanism

Determining the oxidation mechanism of toluene on a non-homogeneous surface is important for the design of catalysts. Three models, Langmuir–Hinshelwood (L-H), Eley–Rideal (E-R), and Mars–van Krevelen (MVK), are generally used to elucidate the deep oxidation kinetics of VOCs [41]. However, the validity of each model depends strongly on the essential nature of catalysts and the type of VOCs. The L-H mechanism means that the reactants are chemically adsorbed on the catalyst surface, and the reaction is carried out through the interaction of molecules or atoms adsorbed on the surface. The E-R model refers to the chemical adsorption of a component in the reactant on the surface of the catalyst, and the reaction is carried out through the interaction of chemisorption atoms or molecules with molecules in the gas phase (or physical adsorption). For the MVK model, the reaction occurs between the adsorbed VOC and the lattice oxygen on the catalyst. First, the VOC reacts with the active oxygen in the catalyst, causing the reduction of the metal oxides in the catalyst, and then the reduced metal oxides are oxidized by the gas phase oxygen. Among them, the MVK model has been widely used for the simulation of the kinetics of toluene oxidation reactions, especially for transition metal oxide materials [103].

In order to match the most appropriate kinetic model, Mi et al. [31] subjected experimental data to linear regression analysis with computational data. By analyzing the reaction rate equation of these models, it was demonstrated that the catalytic oxidation of toluene followed the MVK mechanism. Based on the MVK mechanism, it is widely believed that the catalytic combustion of VOC molecules by transition metal oxides mainly takes place with the participation of lattice oxygen. Furthermore, Liao et al. [104] and Liu et al. [62] reported the main reaction pathway for the oxidation of toluene on the catalyst surface. It was first oxidized to benzyl alcohol, which was immediately converted to benzaldehyde and benzoic acid. Then upon an increase in the reaction temperature, the benzene ring opened to form maleic anhydride. Finally, maleic anhydride was oxidized to CO_2 and H_2O. In detail, the toluene degradation pathway (Figure 3a) can be interpreted as follows: toluene → benzyl alcohol → benzaldehyde → benzoate → phenols → benzoquinone → acid anhydride → CO_2/H_2O [36]. Mi et al. [31] also suggested that toluene first adsorbed

rapidly on the CeO_2 surface to form adsorbed state, which reacted with surface -OH groups to form benzyl species. Benzyl species were further oxidized to benzyloxy, benzaldehyde, and benzoic acid species and finally completely oxidized to H_2O and CO_2. Weak acids can provide more adsorption sites for toluene [36]. As shown in Figure 3b, most toluene molecules after adsorption were attached to reactive oxygen species near oxygen vacancies, and the catalytic degradation process occurred through the abstraction of H atoms from the weakest side chain of the methyl group, then producing benzyl alcohol [68] or benzoyl oxides [27]. In these works, lattice oxygen was consumed to form new oxygen vacancies while surface reactive oxygen was replenished by gas-phase oxygen, thus leading to the regeneration of lattice oxygen and oxygen vacancies. Similar reaction pathways have been found in other studies [42,105,106].

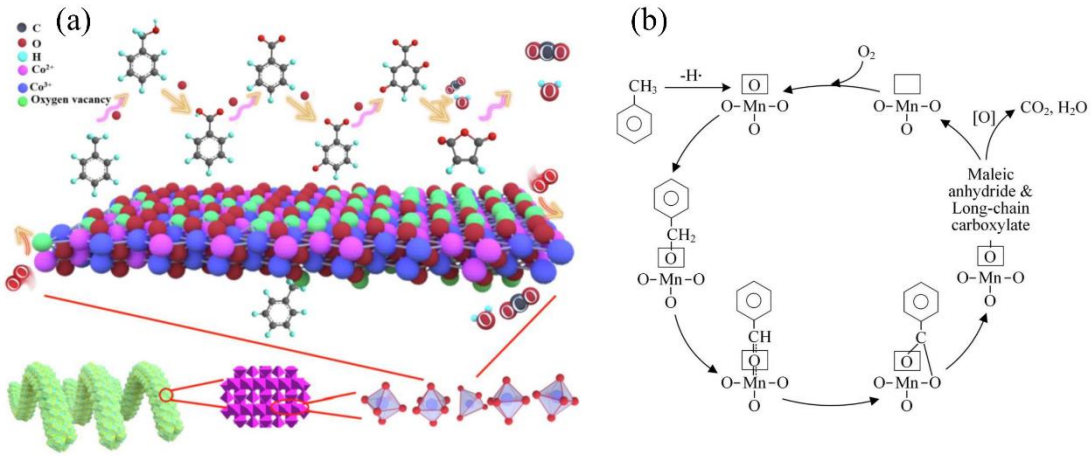

Figure 3. The possible reaction mechanism and pathway over the NH/Tri-Co3O4 (**a**) catalysts [36] and MnO2-Ac (**b**) catalysts [27]. Copyright 2022 and 2020, Elsevier B.V.

5. Mechanism of Synergistic Removal of Toluene and NO

NH_3-SCR and toluene catalytic oxidation both utilize the redox properties of the catalyst, providing a well-established foundation for achieving simultaneous reduction reaction of NO and toluene. However, the synergistic promotion/inhibition between SCR and toluene has proven to be the key to the feasibility of the reaction. In the synergistic elimination of toluene and NO, NH_3-SCR and toluene catalytic oxidation inevitably interact with each other. The interaction between various pollutants is complex and not a simple facilitative or inhibitory effect; it is associated with multiple factors such as reactant concentration, reaction temperature, and catalyst surface characteristics (adsorption properties, surface acidity, redox properties). In order to gain a deeper understanding of the interaction mechanisms of various reactants, clarifying the effects of reaction conditions on the simultaneous elimination performance can help guide the design and regulation of catalysts for the synergistic purification of toluene and NO.

There is no unified understanding of whether there is a synergistic effect between toluene catalytic oxidation and NH_3-SCR. For example, Liu et al. [107] investigated the interaction of simultaneous NO_x and toluene removal over a CeO_2-TiO_2 catalyst which exhibited excellent removal efficiency for both pollutants. The results indicated that NH_3 inhibited toluene oxidation through competitive adsorption, while NO_x promoted its oxidation. Ultimately, the NH_3-SCR process as a whole promoted toluene oxidation. In addition, toluene inhibited NO_x reaction. As shown in Figure 4a, during the simultaneous removal process, the -CH_3 on toluene was first activated by O_2 to produce electrophilic oxygen and the electrophilic oxygen then underwent the toluene catalytic oxidation process, generating a benzoic acid intermediate. In the meantime, gaseous NO was adsorbed on the material surface to form NO_{ad+}, and NO_{ad+} rapidly attacked the offset of the -COOH in the above product to produce m-nitrobenzoic acid. M-nitrobenzoic acid is an electron-rich benzene series that reacts more readily with electrophilic oxygen than benzoic acid.

Subsequently, various carboxylic acids were formed under the action of lattice oxygen due to the opening reaction of the benzene ring. The benzene ring reacted with nitrates adsorbed on the surface to produce organic R-NO_x (containing R-NO, R-ONO, R-NO_2, etc.) and dehydrate the R-NO_x to -CN and -NCO. Finally, these intermediates reacted with nitrates or gas-phase NO/O_2 to form N_2 and CO_2/H_2O. In addition, the reaction temperature affected the redox process of the catalyst. As shown in Figure 4b,c, at lower temperatures (≤200 °C), the O_2 adsorbed on the oxide surface was activated to O_2^-, followed by the oxidation of toluene by O_2^- generating CO_2 and reducing the CeO_2-TiO_2. As temperature increases to 275 °C, the O_2^- is easily converted to O_2^{2-} anion, and Ti^{3+} transfers electrons to Ce^{4+}, eventually forming Ti^{4+}-O_2^{2-}-Ce^{3+} group. It has a strong oxidizing property, which was more favorable for the oxidation of toluene. In addition, Lu et al. [108] found that the existence of NO and NH_3 enhanced the conversion of toluene from 76.6% to 91.8% at 250 °C on MnCe/HZSM-5 catalysts, while the CO_2 selectivity decreased from 60.5% to 34.1%. This was because the NO and NH_3 reacted with intermediates such as aldehydes, carboxylic acids, or phenols to produce nitrile or nitrobenzene during the oxidation of toluene. Nitrile and nitrobenzene were mainly deposited as byproducts on the catalyst surface, which deactivated the catalyst. Specifically, NO competed with toluene on the catalyst for adsorption but promoted toluene oxidation. Conversely, NH_3 promoted toluene adsorption while inhibiting toluene oxidation.

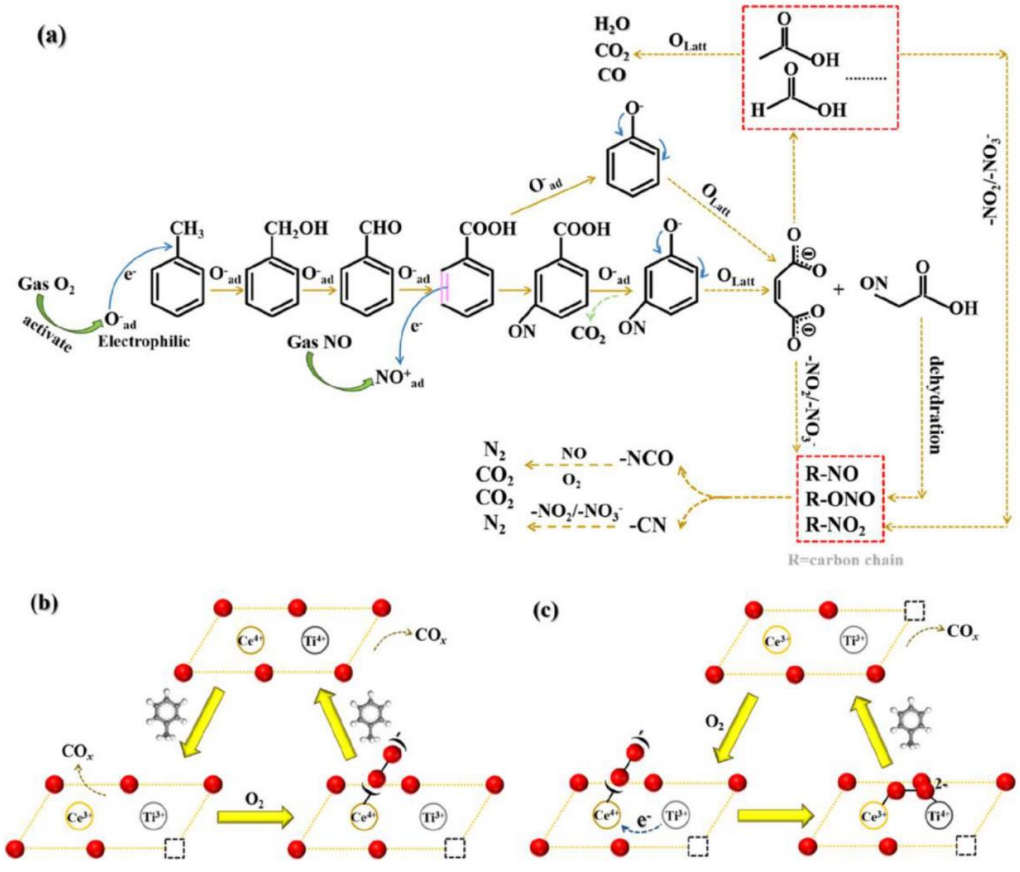

Figure 4. (**a**) Toluene oxidation mechanism in the presence of NO. (**b**) Redox cycle over CeO_2-TiO_2 surface under low-temperature conditions (≤200 °C). (**c**) Redox cycle at high temperatures (≥275 °C) [107]. Copyright 2022, American Chemical Society.

In conclusion, the negative influence of NH_3 on the oxidation of toluene has been confirmed. Reactive oxygen reacts preferentially with NH_3 rather than with the oxidation intermediates of toluene [109]. NH_3 was also thought to promote the formation of nitrile compounds and indirectly inhibit the formation of benzoic acid, maleic acid, and

nitrobenzene, which were key factors in reducing CO_x selectivity in the catalytic oxidation of toluene [110]. Moreover, NO had a facilitative effect on toluene oxidation through the process $C_7H_8 + 18NO = 9N_2 + 7CO_2 + 4H_2O$. Toluene could serve as a reducing agent for NO, facilitating the NH_3-SCR reaction [109]. As shown in Figure 5, Liu et al. [111] found that NO has a facilitating effect on the removal of toluene in the presence of O_2 over the Mn2Fe1 catalyst. However, below 200 °C, toluene had an inhibitory influence on the NO removal. Above 200 °C, the inhibiting effect of toluene on NO diminished. Below 140 °C, NO had a negative influence on toluene oxidation, but this negative effect disappeared as the temperature increased. To some extent, the toluene oxidation reaction was dominant in the process of simultaneous elimination of NO and toluene. O_2 significantly improved the oxidation of toluene by NO, and the presence of strongly oxidizing NO_2 played a positive role in the deep oxidation of toluene. Conversely, the presence of toluene had a negative influence on the deep degradation of NO.

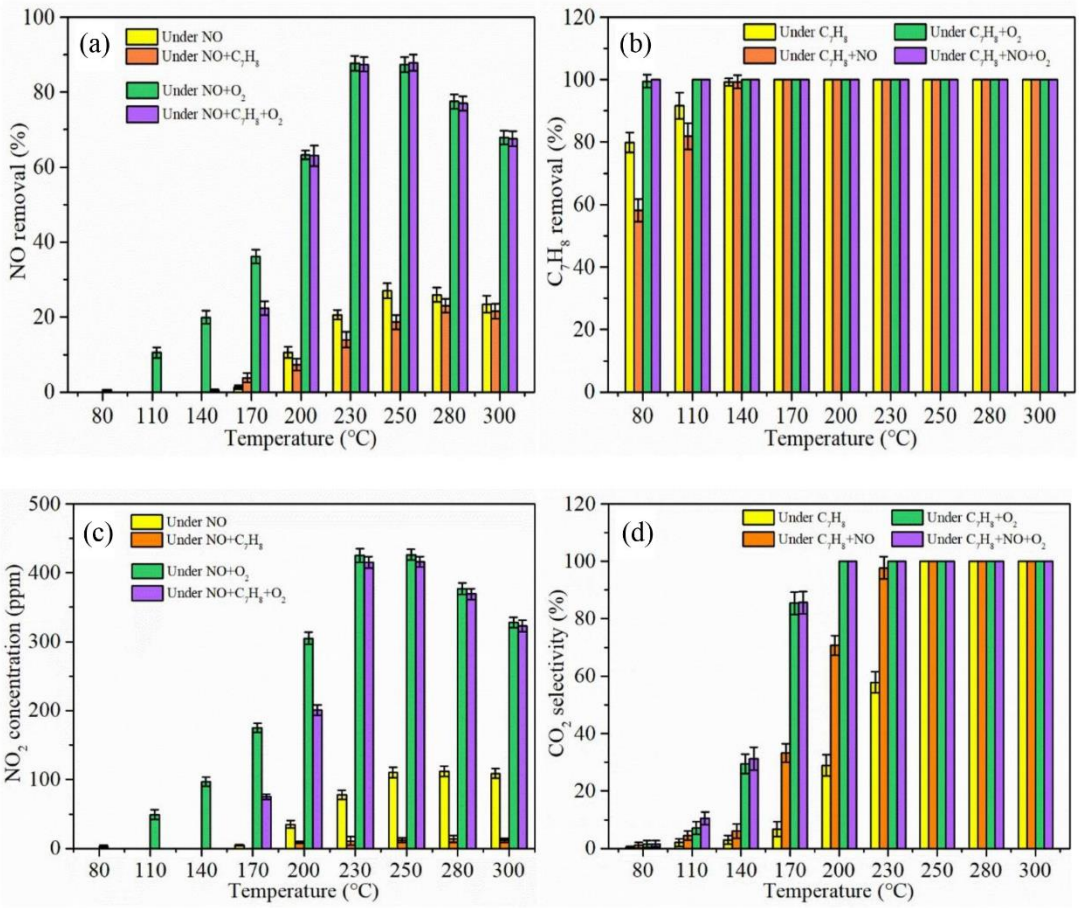

Figure 5. The NO removal (**a**), C_7H_8 removal (**b**), NO_2 concentration (**c**), and CO_2 selectivity (**d**) after 100 min on Mn2Fe1 catalyst [111]. Reaction conditions: [NO] = 500 ppm, [C_7H_8] = 50 ppm, [O_2] = 5 vol%, GHSV = 24,000 h^{-1}, N_2 as balance gas. Copyright 2022, Elsevier B.V.

From the above study, it is clear that there is both a facilitative and an inhibitory influence of toluene on the NH_3-SCR process. The interactions may be related to the reaction temperature or active oxygen. In addition, it has been suggested that porous CuZrCe materials modified with various transition metals (Mn, Fe, Co) affect the reaction mechanism for the synergistic elimination of toluene and NO at low-to-medium temperatures [112]. For CuFeZrCe and CuMnZrCe, toluene showed a slight inhibition of NO conversion owing to the competing adsorption of toluene with NO on active sites. In contrast, the SCR atmosphere promoted the oxidation of toluene owing to the consumption of NO and the generation of emerging Brønsted acid sites during the adsorption of toluene.

For CuCoZrCe, there was a mutual promotion effect under toluene and an SCR atmosphere. The addition of Co provided Co^{3+} as toluene adsorption sites, which counteracted the competitive adsorption of NO and toluene. In particular, Zhao et al. [113] found that there was also a mutual promotion between NO and toluene in the $La_{1-x}Co_xFeO_3$ system. However, for four tunneling structure crystal types (α-MnO_2, β-MnO_2, γ-MnO_2, and δ-MnO_2), there was a mutual inhibition of the synergistic elimination of NO and toluene [114]. Toluene had a significant inhibitory effect on NO conversion, and the existence of NO also increased the conversion temperature of toluene [114]. Furthermore, one of the main problems of Mn-based catalysts was the formation of unfavorable N_2O byproducts in NH_3-SCR, which could destroy the ozone layer [115]. N_2O was primarily generated by NH_3 oxidation and non-catalytic selective reduction (NSCR), which was interpreted as the E-R mechanism and/or the L-H mechanism [115–117]. For the E-R process, the reaction of intermediate NH produced by over-dehydration of adsorbed NH_3 with gaseous NO can generate NHNO, which subsequently decomposes further to N_2O. In the L-H process, adsorbed NH^{4+} reacts with adsorbed NO_3^- to generate NH_4NO_3, which could decompose to N_2O. Toluene affected the redox performance of SCR catalysts and also altered the pathway for N_2O formation in NH_3-SCR. Lu et al. [118] evaluated the effect of toluene on the mechanism of N_2O formation. It was concluded that NSCR dominated below 250 °C and the E-R mechanism dominated at 200 °C. Toluene had a significant inhibition of N_2O formation along with a slight inhibition of NO reaction. This was because toluene inhibited NH_3 peroxidation and N_2O production by NSCR. Both gaseous O_2 and oxygen oxidation of NH_3 on the surface were limited by toluene, resulting in less NH adsorption. However, Ye et al. [119] found that toluene led to more N_2O production in NSCR, which could be due to the generation of oxygen vacancies in the MnCe catalyst.

6. Conclusions and Prospect

This review presented the recent advances and advantages of single metal oxides, multi-oxide composites, and supported metal oxide catalysts for the catalytic elimination of a typical VOC (toluene). The activities of different catalysts were summarized and compared, and the critical factors influencing the degradation of toluene were revealed. The kinetic model, toluene oxidation mechanism, and synergistic reaction mechanism between toluene oxidation and NH_3-SCR were also investigated. Among various catalysts, Mn-based catalysts usually have excellent oxidation activity, while supported metal oxide catalysts have high stability. The catalytic activity is influenced by the type of active phase and carrier, the type of active metal precursor, the loading amount, the preparation method, and the intrinsic properties of metal oxides (dispersion, crystal structure, microscopic morphology, valence, reduction, reactive oxygen species, etc.). The multi-metal oxides in general have higher catalytic activity than similar individual metal oxides. The enhanced interaction between the active component and the loaded/doped component becomes a bottleneck limiting catalyst development. The synergistic promotion/inhibition between toluene and NO, NH_3, heavy metals, etc., was shown to be the key to the synergistic reaction control technology.

Despite the remarkable progress, there are still some outstanding issues that need attention in future research:

(1) Industrial monolithic catalysts with improved VOC reduction should be further developed. Surface modification methods should have easy preparation processes, large scale, and precisely controlled conditions.

(2) Catalyst deactivation is a major defect in industrial applications. The iron sintering flue gas environment is often very complex, and trace contaminants such as water vapor, SO_2, chlorine-containing compounds, and heavy metals may be present simultaneously. Therefore, catalysts with high activity, stability, and resistance to poisoning need to be designed. In addition, further understanding of the sources of poisoning or deactivation of different catalysts can enable industrially viable regeneration tech-

niques by establishing correlations between the surface properties of the parent body and its catalytic activity.

(3) In the simultaneous elimination of VOCs and NO, the reactions between NH_3/NO, oxygen, and toluene over catalysts are still intricate and in their infancy. Theoretical calculations can be used to understand the reaction pathways, intermediate species migration, and conversion mechanisms for the simultaneous elimination of VOCs and NO at the molecular level.

Author Contributions: Q.S.: methodology, writing—original draft, investigation, visualization. D.K.: investigation, formal analysis, validation. Y.W.: validation, writing—original draft. X.Z.: funding acquisition, resources, conceptualization. All authors have read and agreed to the published version of the manuscript.

Funding: The research was supported by Joint Funds of the National Natural Science Foundation of China (U20A20302), Innovative Group Projects in Hebei Province (E2021202006), Key R&D Projects in Hebei Province (20373701D), and Project of Great Transformation of Scientific and Technical Research in Hebei Province (21283701Z).

Data Availability Statement: Not applicable.

Conflicts of Interest: The authors declare no conflict of interest.

References

1. Zhang, Y.; Zheng, J. Blue paper on the prevention and control of atmospheric ozone pollution in China: Professional committee of ozone pollution control. *Chin. Soc. Environ. Sci.* **2020**. Available online: https://mp.weixin.qq.com/s/y9CJhur7v18aBhYcOTvgQA (accessed on 15 February 2023).
2. Ding, A.; Huang, X.; Nie, W.; Chi, X.; Xu, Z.; Zheng, L.; Xu, Z.; Xie, Y.; Qi, X.; Shen, Y.; et al. Significant reduction of $PM_{2.5}$ in eastern China due to regional-scale emission control: Evidence from SORPES in 2011–2018. *Atmos. Chem. Phys.* **2019**, *19*, 11791–11801. [CrossRef]
3. Li, B.; Ho, S.S.H.; Li, X.; Guo, L.; Chen, A.; Hu, L.; Yang, Y.; Chen, D.; Lin, A.; Fang, X. A comprehensive review on anthropogenic volatile organic compounds (VOCs) emission estimates in China: Comparison and outlook. *Environ. Int.* **2021**, *156*, 106710. [CrossRef] [PubMed]
4. Wu, R.; Xie, S. Spatial Distribution of Ozone Formation in China Derived from Emissions of Speciated Volatile Organic Compounds. *Environ. Sci. Technol.* **2017**, *51*, 2574–2583. [CrossRef]
5. Li, J.; Zhou, Y.; Simayi, M.; Deng, Y.; Xie, S. Spatial-temporal variations and reduction potentials of volatile organic compound emissions from the coking industry in China. *J. Cleaner Prod.* **2019**, *214*, 224–235. [CrossRef]
6. Li, M.; Zhang, Q.; Zheng, B.; Tong, D.; Lei, Y.; Liu, F.; Hong, C.; Kang, S.; Yan, L.; Zhang, Y.; et al. Persistent growth of anthropogenic non-methane volatile organic compound (NMVOC) emissions in China during 1990–2017: Drivers, speciation and ozone formation potential. *Atmos. Chem. Phys.* **2019**, *19*, 8897–8913. [CrossRef]
7. Hu, H.; Zhang, Y.; Rao, X.; Jin, Y. Impact of Technology Innovation on Air Quality-An Empirical Study on New Energy Vehicles in China. *Int. J. Environ. Res. Public Health* **2021**, *18*, 4025. [CrossRef]
8. Kieush, L.; Koveria, A.; Boyko, M.; Yaholnyk, M.; Hrubiak, A.; Molchanov, L.; Moklyak, V. Influence of biocoke on iron ore sintering performance and strength properties of sinter. *Min. Miner. Depos.* **2022**, *16*, 55–63. [CrossRef]
9. Peng, Y.; Yang, Q.; Wang, L.; Wang, S.; Li, J.; Zhang, X.; Zhang, S.; Zhao, H.; Zhang, B.; Wang, C.; et al. VOC emissions of coal-fired power plants in China based on life cycle assessment method. *Fuel* **2021**, *292*, 120325. [CrossRef]
10. Wang, Y.; Ding, L.; Shi, Q.; Liu, S.; Qian, L.; Yu, Z.; Wang, H.; Lei, J.; Gao, Z.; Long, H.; et al. Volatile organic compounds (VOC) emissions control in iron ore sintering process: Recent progress and future development. *Chem. Eng. J.* **2022**, *448*, 137601. [CrossRef]
11. Ma, L.-Y.; Li, Z.-Y. Research on the Effect of Chinese Margin Trading on Market Risk: Based on GJR Model and Filtered Historical Simulation. *Appl. Econ. and Fin.* **2017**, *4*, 84. [CrossRef]
12. Li, Y.; Wang, Y.; Liu, H.; Sun, W.; Ding, B.; Zhao, Y.; Chen, P.; Zhu, L.; Li, Z.; Li, N.; et al. Urine proteome of COVID-19 patients. *Urine* **2020**, *2*, 1–8. [CrossRef] [PubMed]
13. Li, J.; He, X.; Pei, B.; Li, X.; Ying, D.; Wang, Y.; Jia, J. The ignored emission of volatile organic compounds from iron ore sinter process. *J. Environ. Sci.* **2019**, *77*, 282–290. [CrossRef] [PubMed]
14. Qian, L.; Chun, T.; Long, H.; Li, J.; Di, Z.; Meng, Q.; Wang, P. Emission reduction research and development of PCDD/Fs in the iron ore sintering. *Process Saf. Environ. Prot.* **2018**, *117*, 82–91. [CrossRef]
15. Wang, H.; Yuan, B.; Hao, R.; Zhao, Y.; Wang, X. A critical review on the method of simultaneous removal of multi-air-pollutant in flue gas. *Chem. Eng. J.* **2019**, *378*, 122155. [CrossRef]

16. Liu, J.; Yuan, Y.; Zhang, J.; He, Z.; Yu, Y. Combustion Kinetics Characteristics of Solid Fuel in the Sintering Process. *Processes* **2020**, *8*, 475. [CrossRef]
17. Wang, R.; Wang, X.; Cheng, S.; Wang, K.; Cheng, L.; Zhu, J.; Zheng, H.; Duan, W. Emission characteristics and reactivity of volatile organic compounds from typical high-energy-consuming industries in North China. *Sci. Total Environ.* **2022**, *809*, 151134. [CrossRef] [PubMed]
18. Wu, X.; Han, R.; Liu, Q.; Su, Y.; Lu, S.; Yang, L.; Song, C.; Ji, N.; Ma, D.; Lu, X. A review of confined-structure catalysts in the catalytic oxidation of VOCs: Synthesis, characterization, and applications. *Catal. Sci. Technol.* **2021**, *11*, 5374–5387. [CrossRef]
19. Meng, Q.; Wang, W.; Weng, X.; Liu, Y.; Wang, H.; Wu, Z. Active Oxygen Species in $La_{n+1}Ni_nO_{3n+1}$ Layered Perovskites for Catalytic Oxidation of Toluene and Methane. *J. Phys. Chem. C* **2016**, *120*, 3259–3266. [CrossRef]
20. Hermiaa, J.; Vigneron, S. Catalytic incineration for odour abatement and VOC destruction. *Catal. Today* **1993**, *17*, 349–356. [CrossRef]
21. Kang, D.; Bian, Y.; Shi, Q.; Wang, J.; Yuan, P.; Shen, B. A Review of Synergistic Catalytic Removal of Nitrogen Oxides and Chlorobenzene from Waste Incinerators. *Catalysts* **2022**, *12*, 1360. [CrossRef]
22. Piumetti, M.; Fino, D.; Russo, N. Mesoporous manganese oxides prepared by solution combustion synthesis as catalysts for the total oxidation of VOCs. *Appl. Catal. B Environ.* **2015**, *163*, 277–287. [CrossRef]
23. Li, K.; Chen, C.; Zhang, H.; Hu, X.; Sun, T.; Jia, J. Effects of phase structure of MnO_2 and morphology of δ-MnO_2 on toluene catalytic oxidation. *Appl. Surf. Sci.* **2019**, *496*, 143662. [CrossRef]
24. Huang, J.; Fang, R.; Sun, Y.; Li, J.; Dong, F. Efficient α-MnO_2 with (2 1 0) facet exposed for catalytic oxidation of toluene at low temperature: A combined in-situ DRIFTS and theoretical investigation. *Chemosphere* **2021**, *263*, 128103. [CrossRef]
25. Chen, L.; Liu, Y.; Fang, X.; Cheng, Y. Simple strategy for the construction of oxygen vacancies on α-MnO_2 catalyst to improve toluene catalytic oxidation. *J. Hazard. Mater.* **2021**, *409*, 125020. [CrossRef] [PubMed]
26. Wang, F.; Dai, H.; Deng, J.; Bai, G.; Ji, K.; Liu, Y. Manganese oxides with rod-, wire-, tube-, and flower-like morphologies: Highly effective catalysts for the removal of toluene. *Environ. Sci. Technol.* **2012**, *46*, 4034–4041. [CrossRef]
27. Lyu, Y.; Li, C.; Du, X.; Zhu, Y.; Zhang, Y.; Li, S. Catalytic oxidation of toluene over MnO_2 catalysts with different Mn (II) precursors and the study of reaction pathway. *Fuel* **2020**, *262*, 116610. [CrossRef]
28. Zhang, X.; Zhao, H.; Song, Z.; Liu, W.; Zhao, J.; Ma, Z.; Zhao, M.; Xing, Y. Insight into the effect of oxygen species and Mn chemical valence over MnO on the catalytic oxidation of toluene. *Appl. Surf. Sci.* **2019**, *493*, 9–17. [CrossRef]
29. Hu, F.; Chen, J.; Peng, Y.; Song, H.; Li, K.; Li, J. Novel nanowire self-assembled hierarchical CeO_2 microspheres for low temperature toluene catalytic combustion. *Chem. Eng. J.* **2018**, *331*, 425–434. [CrossRef]
30. Feng, Z.; Ren, Q.; Peng, R.; Mo, S.; Zhang, M.; Fu, M.; Chen, L.; Ye, D. Effect of CeO_2 morphologies on toluene catalytic combustion. *Catal. Today* **2019**, *332*, 177–182. [CrossRef]
31. Mi, R.; Li, D.; Hu, Z.; Yang, R.T. Morphology Effects of CeO_2 Nanomaterials on the Catalytic Combustion of Toluene: A Combined Kinetics and Diffuse Reflectance Infrared Fourier Transform Spectroscopy Study. *ACS Catal.* **2021**, *11*, 7876–7889. [CrossRef]
32. Yan, D.; Mo, S.; Sun, Y.; Ren, Q.; Feng, Z.; Chen, P.; Wu, J.; Fu, M.; Ye, D. Morphology-activity correlation of electrospun CeO_2 for toluene catalytic combustion. *Chemosphere* **2020**, *247*, 125860. [CrossRef] [PubMed]
33. Chen, X.; Chen, X.; Yu, E.; Cai, S.; Jia, H.; Chen, J.; Liang, P. In situ pyrolysis of Ce-MOF to prepare CeO_2 catalyst with obviously improved catalytic performance for toluene combustion. *Chem. Eng. J.* **2018**, *344*, 469–479. [CrossRef]
34. Ren, Q.; Feng, Z.; Mo, S.; Huang, C.; Li, S.; Zhang, W.; Chen, L.; Fu, M.; Wu, J.; Ye, D. 1D-Co_3O_4, 2D-Co_3O_4, 3D-Co_3O_4 for catalytic oxidation of toluene. *Catal. Today* **2019**, *332*, 160–167. [CrossRef]
35. Ren, Q.; Mo, S.; Peng, R.; Feng, Z.; Zhang, M.; Chen, L.; Fu, M.; Wu, J.; Ye, D. Controllable synthesis of 3D hierarchical Co_3O_4 nanocatalysts with various morphologies for the catalytic oxidation of toluene. *J. Mater. Chem. A* **2018**, *6*, 498–509. [CrossRef]
36. Han, W.; Dong, F.; Han, W.; Yao, J.; Meng, Y.; Tang, Z. A new strategy for designing highly efficient Co_3O_4 catalyst with the molecular space configurations for toluene catalytic combustion. *Chem. Eng. J.* **2022**, *435*, 134953. [CrossRef]
37. Zhao, J.; Tang, Z.; Dong, F.; Zhang, J. Controlled porous hollow Co_3O_4 polyhedral nanocages derived from metal-organic frameworks (MOFs) for toluene catalytic oxidation. *Mol. Catal.* **2019**, *463*, 77–86. [CrossRef]
38. Lei, J.; Wang, S.; Li, J. Mesoporous Co_3O_4 derived from Co-MOFs with different morphologies and ligands for toluene catalytic oxidation. *Chem. Eng. Sci.* **2020**, *220*, 115654. [CrossRef]
39. Yang, R.; Fan, Y.; Ye, R.; Tang, Y.; Cao, X.; Yin, Z.; Zeng, Z. MnO_2 -Based Materials for Environmental Applications. *Adv. Mater.* **2021**, *33*, e2004862. [CrossRef]
40. Hou, Z.; Feng, J.; Lin, T.; Zhang, H.; Zhou, X.; Chen, Y. The performance of manganese-based catalysts with $Ce_{0.65}Zr_{0.35}O_2$ as support for catalytic oxidation of toluene. *Appl. Surf. Sci.* **2018**, *434*, 82–90. [CrossRef]
41. He, C.; Cheng, J.; Zhang, X.; Douthwaite, M.; Pattisson, S.; Hao, Z. Recent Advances in the Catalytic Oxidation of Volatile Organic Compounds: A Review Based on Pollutant Sorts and Sources. *Chem. Rev.* **2019**, *119*, 4471–4568. [CrossRef]
42. Su, Z.; Yang, W.; Wang, C.; Xiong, S.; Cao, X.; Peng, Y.; Si, W.; Weng, Y.; Xue, M.; Li, J. Roles of Oxygen Vacancies in the Bulk and Surface of CeO_2 for Toluene Catalytic Combustion. *Environ. Sci. Technol.* **2020**, *54*, 12684–12692. [CrossRef]
43. Li, Y.; Chen, T.; Zhao, S.; Wu, P.; Chong, Y.; Li, A.; Zhao, Y.; Chen, G.; Jin, X.; Qiu, Y.; et al. Engineering Cobalt Oxide with Coexisting Cobalt Defects and Oxygen Vacancies for Enhanced Catalytic Oxidation of Toluene. *ACS Catal.* **2022**, *12*, 4906–4917. [CrossRef]

44. Liu, W.; Liu, R.; Zhang, X. Controllable synthesis of 3D hierarchical Co_3O_4 catalysts and their excellent catalytic performance for toluene combustion. *Appl. Surf. Sci.* **2020**, *507*, 145174. [CrossRef]
45. Zhang, X.; Shi, Q.; Shen, B.; Hu, Z.; Zhang, X. MIL-100(Fe) supported Mn-based catalyst and its behavior in Hg^0 removal from flue gas. *J. Hazard. Mater.* **2019**, *381*, 121003. [CrossRef] [PubMed]
46. Lei, J.; Wang, S.; Li, J.; Xu, Y.; Li, S. Different effect of Y (Y = Cu, Mn, Fe, Ni) doping on Co_3O_4 derived from Co-MOF for toluene catalytic destruction. *Chem. Eng. Sci.* **2022**, *251*, 117436. [CrossRef]
47. Yan, Q.; Li, X.; Zhao, Q.; Chen, G. Shape-controlled fabrication of the porous Co_3O_4 nanoflower clusters for efficient catalytic oxidation of gaseous toluene. *J. Hazard. Mater.* **2012**, *209–210*, 385–391. [CrossRef]
48. Shi, Q.; Shen, B.; Zhang, X.; Lyu, H.; Wang, J.; Li, S.; Kang, D. Insights into synergistic oxidation mechanism of Hg^0 and chlorobenzene over $MnCo_2O_4$ microsphere with oxygen vacancy and acidic site. *J. Hazard. Mater.* **2023**, *443*, 130179. [CrossRef]
49. Wu, P.; Jin, X.; Qiu, Y.; Ye, D. Recent Progress of Thermocatalytic and Photo/Thermocatalytic Oxidation for VOCs Purification over Manganese-based Oxide Catalysts. *Environ. Sci. Technol.* **2021**, *55*, 4268–4286. [CrossRef]
50. Hu, W.; Huang, J.; Xu, J.; Cheng, S.; Lyu, Y.; Xie, D.; Wang, Z. Insights into the superior performance of mesoporous MOFs-derived Cu-Mn oxides for toluene total catalytic oxidation. *Fuel Process. Technol.* **2022**, *236*, 107424. [CrossRef]
51. Wei, G.; Zhang, Q.; Zhang, D.; Wang, J.; Tang, T.; Wang, H.; Liu, X.; Song, Z.; Ning, P. The influence of annealing temperature on copper-manganese catalyst towards the catalytic combustion of toluene: The mechanism study. *Appl. Surf. Sci.* **2019**, *497*, 143777. [CrossRef]
52. Liu, W.; Wang, S.; Cui, R.; Song, Z.; Zhang, X. Enhancement of catalytic combustion of toluene over CuMnOx hollow spheres prepared by oxidation method. *Microporous Mesoporous Mater.* **2021**, *326*, 111370. [CrossRef]
53. Liu, W.; Xiang, W.; Chen, X.; Song, Z.; Gao, C.; Tsubaki, N.; Zhang, X. A novel strategy to adjust the oxygen vacancy of CuO/MnO_2 catalysts toward the catalytic oxidation of toluene. *Fuel* **2022**, *312*, 122975. [CrossRef]
54. Li, J.; Zhang, W.; Li, C.; He, C. Efficient catalytic degradation of toluene at a readily prepared Mn-Cu catalyst: Catalytic performance and reaction pathway. *J. Colloid Interface Sci.* **2021**, *591*, 396–408. [CrossRef] [PubMed]
55. Luo, M.; Cheng, Y.; Peng, X.; Pan, W. Copper modified manganese oxide with tunnel structure as efficient catalyst for low-temperature catalytic combustion of toluene. *Chem. Eng. J.* **2019**, *369*, 758–765. [CrossRef]
56. Du, J.; Qu, Z.; Dong, C.; Song, L.; Qin, Y.; Huang, N. Low-temperature abatement of toluene over Mn-Ce oxides catalysts synthesized by a modified hydrothermal approach. *Appl. Surf. Sci.* **2018**, *433*, 1025–1035. [CrossRef]
57. Zhang, X.; Zhao, J.; Song, Z.; Liu, W.; Zhao, H.; Zhao, M.; Xing, Y.; Ma, Z.; Du, H. The catalytic oxidation performance of toluene over the Ce-Mn-Ox catalysts: Effect of synthetic routes. *J. Colloid Interface Sci.* **2020**, *562*, 170–181. [CrossRef]
58. Liao, Y.; Fu, M.; Chen, L.; Wu, J.; Huang, B.; Ye, D. Catalytic oxidation of toluene over nanorod-structured Mn–Ce mixed oxides. *Catal. Today* **2013**, *216*, 220–228. [CrossRef]
59. Li, L.; Jing, F.; Yan, J.; Jing, J.; Chu, W. Highly effective self-propagating synthesis of CeO_2-doped MnO_2 catalysts for toluene catalytic combustion. *Catal. Today* **2017**, *297*, 167–172. [CrossRef]
60. Dong, C.; Qu, Z.; Qin, Y.; Fu, Q.; Sun, H.; Duan, X. Revealing the Highly Catalytic Performance of Spinel $CoMn_2O_4$ for Toluene Oxidation: Involvement and Replenishment of Oxygen Species Using In Situ Designed-TP Techniques. *ACS Catal.* **2019**, *9*, 6698–6710. [CrossRef]
61. Qu, Z.; Gao, K.; Fu, Q.; Qin, Y. Low-temperature catalytic oxidation of toluene over nanocrystal-like Mn–Co oxides prepared by two-step hydrothermal method. *Catal. Commun.* **2014**, *52*, 31–35. [CrossRef]
62. Liu, W.; Xiang, W.; Guan, N.; Cui, R.; Cheng, H.; Chen, X.; Song, Z.; Zhang, X.; Zhang, Y. Enhanced catalytic performance for toluene purification over Co_3O_4/MnO_2 catalyst through the construction of different Co_3O_4/MnO_2 interface. *Sep. Purif. Technol.* **2021**, *278*, 119590. [CrossRef]
63. Ren, Q.; Mo, S.; Fan, J.; Feng, Z.; Zhang, M.; Chen, P.; Gao, J.; Fu, M.; Chen, L.; Wu, J.; et al. Enhancing catalytic toluene oxidation over MnO_2@Co_3O_4 by constructing a coupled interface. *Chin. J. Catal.* **2020**, *41*, 1873–1883. [CrossRef]
64. Dong, Y.; Zhao, J.; Zhang, J.-Y.; Chen, Y.; Yang, X.; Song, W.; Wei, L.; Li, W. Synergy of Mn and Ni enhanced catalytic performance for toluene combustion over Ni-doped α-MnO_2 catalysts. *Chem. Eng. J.* **2020**, *388*, 124244. [CrossRef]
65. Yang, X.; Yu, X.; Jing, M.; Song, W.; Liu, J.; Ge, M. Defective $Mn_xZr_{1-x}O_2$ solid solution for the catalytic oxidation of toluene: Insights into the oxygen vacancy contribution. *ACS Appl. Mater. Interfaces* **2018**, *11*, 730–739. [CrossRef] [PubMed]
66. Li, W.; Gao, G.; Wang, L.; Xu, H.; Huang, W.; Yan, N.; Qu, Z. Dual confinement strategy based on metal-organic frameworks to synthesize MnOx@ZrO_2 catalysts for toluene catalytic oxidation. *Fuel* **2022**, *320*, 123983. [CrossRef]
67. Zhou, G.; Lan, H.; Yang, X.; Du, Q.; Xie, H.; Fu, M. Effects of the structure of Ce-Cu catalysts on the catalytic combustion of toluene in air. *Ceram. Int.* **2013**, *39*, 3677–3683. [CrossRef]
68. Song, B.; Li, C.; Du, X.; Li, S.; Zhang, Y.; Lyu, Y.; Zhou, Q. Superior performance of Cu-Ce binary oxides for toluene catalytic oxidation: Cu-Ce synergistic effect and reaction pathways. *Fuel* **2021**, *306*, 121654. [CrossRef]
69. Carabineiro, S.; Chen, X.; Konsolakis, M.; Psarras, A.; Tavares, P.; Órfão, J.; Pereira, M.; Figueiredo, J.L. Catalytic oxidation of toluene on Ce–Co and La–Co mixed oxides synthesized by exotemplating and evaporation methods. *Catal. Today* **2015**, *244*, 161–171. [CrossRef]
70. Ismail, A.; Li, M.; Zahid, M.; Fan, L.; Zhang, C.; Li, Z.; Zhu, Y. Effect of strong interaction between Co and Ce oxides in $Co_xCe_{1-x}O_{2-\delta}$ oxides on its catalytic oxidation of toluene. *Mol. Catal.* **2021**, *502*, 111356. [CrossRef]

71. Xu, W.; Chen, X.; Chen, J.; Jia, H. Bimetal oxide CuO/Co_3O_4 derived from Cu ions partly-substituted framework of ZIF-67 for toluene catalytic oxidation. *J. Hazard. Mater.* **2021**, *403*, 123869. [CrossRef] [PubMed]
72. Sihaib, Z.; Puleo, F.; Garcia-Vargas, J.; Retailleau, L.; Descorme, C.; Liotta, L.; Valverde, J.; Gil, S.; Giroir-Fendler, A. Manganese oxide-based catalysts for toluene oxidation. *Appl. Catal. B Environ.* **2017**, *209*, 689–700. [CrossRef]
73. Zhang, C.; Guo, Y.; Guo, Y.; Lu, G.; Boreave, A.; Retailleau, L.; Baylet, A.; Giroir-Fendler, A. $LaMnO_3$ perovskite oxides prepared by different methods for catalytic oxidation of toluene. *Appl. Catal. B Environ.* **2014**, *148–149*, 490–498. [CrossRef]
74. Liu, L.; Sun, J.; Ding, J.; Zhang, Y.; Jia, J.; Sun, T. Catalytic Oxidation of VOCs over $SmMnO_3$ Perovskites: Catalyst Synthesis, Change Mechanism of Active Species, and Degradation Path of Toluene. *Inorg. Chem.* **2019**, *58*, 14275–14283. [CrossRef]
75. Chen, S.; Hao, Y.; Chen, R.; Su, Z.; Chen, T. Hollow multishelled spherical $PrMnO_3$ perovskite catalyst for efficient catalytic oxidation of CO and toluene. *J. Alloys Compd.* **2021**, *861*, 158584. [CrossRef]
76. Wang, Y.; Xue, Y.; Zhao, C.; Zhao, D.; Liu, F.; Wang, K.; Dionysiou, D.D. Catalytic combustion of toluene with $La_{0.8}Ce_{0.2}MnO_3$ supported on CeO_2 with different morphologies. *Chem. Eng. J.* **2016**, *300*, 300–305. [CrossRef]
77. Yang, J.; Li, L.; Yang, X.; Song, S.; Li, J.; Jing, F.; Chu, W. Enhanced catalytic performances of in situ-assembled $LaMnO_3/\delta$-MnO_2 hetero-structures for toluene combustion. *Catal. Today* **2019**, *327*, 19–27. [CrossRef]
78. Suárez-Vázquez, S.; Gil, S.; García-Vargas, J.; Cruz-López, A.; Giroir-Fendler, A. Catalytic oxidation of toluene by $SrTi_{1-X}B_XO_3$ (B = Cu and Mn) with dendritic morphology synthesized by one pot hydrothermal route. *Appl. Catal. B Environ.* **2018**, *223*, 201–208. [CrossRef]
79. Dula, R.; Janik, R.; Machej, T.; Stoch, J.; Grabowski, R.; Serwicka, E.M. Mn-containing catalytic materials for the total combustion of toluene: The role of Mn localisation in the structure of LDH precursor. *Catal. Today* **2007**, *119*, 327–331. [CrossRef]
80. Lu, H.; Kong, X.; Huang, H.; Zhou, Y.; Chen, Y. Cu-Mn-Ce ternary mixed-oxide catalysts for catalytic combustion of toluene. *J. Environ. Sci.* **2015**, *32*, 102–107. [CrossRef]
81. Hu, F.; Chen, J.; Zhao, S.; Li, K.; Si, W.; Song, H.; Li, J. Toluene catalytic combustion over copper modified $Mn_{0.5}Ce_{0.5}O_x$ solid solution sponge-like structures. *Appl. Catal. A* **2017**, *540*, 57–67. [CrossRef]
82. Wang, D.; Yang, Q.; Yang, G.; Xiong, S.; Li, X.; Peng, Y.; Li, J.; Crittenden, J. Rational tuning towards A/B-sites double-occupying cobalt on tri-metallic spinel: Insights into its catalytic activity on toluene catalytic oxidation. *Chem. Eng. J.* **2020**, *399*, 125792. [CrossRef]
83. Wang, Y.; Xue, R.; Zhao, C.; Liu, F.; Liu, C.; Han, F. Effects of Ce in the catalytic combustion of toluene on $Cu_xCe_{1-x}Fe_2O_4$. *Colloids Surf. A* **2018**, *540*, 90–97. [CrossRef]
84. Liu, L.; Li, J.; Zhang, H.; Li, L.; Zhou, P.; Meng, X.; Guo, M.; Jia, J.; Sun, T. In situ fabrication of highly active γ-$MnO_2/SmMnO_3$ catalyst for deep catalytic oxidation of gaseous benzene, ethylbenzene, toluene, and o-xylene. *J. Hazard. Mater.* **2019**, *362*, 178–186. [CrossRef] [PubMed]
85. Yu, D.; Liu, Y.; Wu, Z. Low-temperature catalytic oxidation of toluene over mesoporous MnO–CeO_2/TiO_2 prepared by sol–gel method. *Catal. Commun.* **2010**, *11*, 788–791. [CrossRef]
86. He, Y.; Rui, Z.; Ji, H. In situ DRIFTS study on the catalytic oxidation of toluene over V_2O_5/TiO_2 under mild conditions. *Catal. Commun.* **2011**, *14*, 77–81. [CrossRef]
87. Pozan, G.S. Effect of support on the catalytic activity of manganese oxide catalyts for toluene combustion. *J. Hazard. Mater.* **2012**, *221–222*, 124–130. [CrossRef]
88. Wang, H.; Lu, Y.; Han, Y.; Lu, C.; Wan, H.; Xu, Z.; Zheng, S. Enhanced catalytic toluene oxidation by interaction between copper oxide and manganese oxide in Cu-O-Mn/γ-Al_2O_3 catalysts. *Appl. Surf. Sci.* **2017**, *420*, 260–266. [CrossRef]
89. Saqer, S.; Kondarides, D.; Verykios, X.E. Catalytic Activity of Supported Platinum and Metal Oxide Catalysts for Toluene Oxidation. *Top. Catal.* **2009**, *52*, 517–527. [CrossRef]
90. Li, X.; Wang, L.; Xia, Q.; Liu, Z.; Li, Z. Catalytic oxidation of toluene over copper and manganese based catalysts: Effect of water vapor. *Catal. Commun.* **2011**, *14*, 15–19. [CrossRef]
91. Wang, Z.; Xie, K.; Zheng, J.; Zuo, S. Studies of sulfur poisoning process via ammonium sulfate on MnO_2/γ-Al_2O_3 catalyst for catalytic combustion of toluene. *Appl. Catal. B Environ.* **2021**, *298*, 120595. [CrossRef]
92. Saqer, S.; Kondarides, D.; Verykios, X. Catalytic oxidation of toluene over binary mixtures of copper, manganese and cerium oxides supported on γ-Al_2O_3. *Appl. Catal. B Environ.* **2011**, *103*, 275–286. [CrossRef]
93. Palacio, L.; Silva, E.; Catalao, R.; Silva, J.; Hoyos, D.; Ribeiro, F.; Ribeiro, M.F. Performance of supported catalysts based on a new copper vanadate-type precursor for catalytic oxidation of toluene. *J. Hazard. Mater.* **2008**, *153*, 628–634. [CrossRef] [PubMed]
94. Chen, C.; Wang, X.; Zhang, J.; Bian, C.; Pan, S.; Chen, F.; Meng, X.; Zheng, X.; Gao, X.; Xiao, F.-S. Superior performance in catalytic combustion of toluene over mesoporous ZSM-5 zeolite supported platinum catalyst. *Catal. Today* **2015**, *258*, 190–195. [CrossRef]
95. Zhang, C.; Huang, H.; Li, G.; Wang, L.; Song, L.; Li, X. Zeolitic acidity as a promoter for the catalytic oxidation of toluene over MnO_x/HZSM-5 catalysts. *Catal. Today* **2019**, *327*, 374–381. [CrossRef]
96. Rokicińska, A.; Drozdek, M.; Dudek, B.; Gil, B.; Michorczyk, P.; Brouri, D.; Dzwigaj, S.; Kuśtrowski, P. Cobalt-containing BEA zeolite for catalytic combustion of toluene. *Appl. Catal. B Environ.* **2017**, *212*, 59–67. [CrossRef]
97. Soylu, G.; Özçelik, Z.; Boz, İ. Total oxidation of toluene over metal oxides supported on a natural clinoptilolite-type zeolite. *Chem. Eng. J.* **2010**, *162*, 380–387. [CrossRef]
98. Li, W.; Zhuang, M.; Wang, J.X. Catalytic combustion of toluene on Cu-Mn/MCM-41 catalysts: Influence of calcination temperature and operating conditions on the catalytic activity. *Catal. Today* **2008**, *137*, 340–344. [CrossRef]

99. Ma, W.; Huang, Q.; Xu, Y.; Chen, Y.; Zhu, S.; Shen, S.B. Catalytic combustion of toluene over Fe–Mn mixed oxides supported on cordierite. *Ceram. Int.* **2013**, *39*, 277–281. [CrossRef]
100. Liang, X.; Qi, F.; Liu, P.; Wei, G.; Su, X.; Ma, L.; He, H.; Lin, X.; Xi, Y.; Zhu, J.; et al. Performance of Ti-pillared montmorillonite supported Fe catalysts for toluene oxidation: The effect of Fe on catalytic activity. *Appl. Clay Sci.* **2016**, *132–133*, 96–104. [CrossRef]
101. Cheng, Z.; Chen, Z.; Li, J.; Zuo, S.; Yang, P. Mesoporous silica-pillared clays supported nanosized Co_3O_4-CeO_2 for catalytic combustion of toluene. *Appl. Surf. Sci.* **2018**, *459*, 32–39. [CrossRef]
102. Bakardjieva, S.; Šubrt, J.; Štengl, V.; Dianez, M.; Sayagues, M.J. Photoactivity of anatase–rutile TiO_2 nanocrystalline mixtures obtained by heat treatment of homogeneously precipitated anatase. *Appl. Catal. B Environ.* **2005**, *58*, 193–202. [CrossRef]
103. Lin, F.; Xiang, L.; Zhang, Z.; Li, N.; Yan, B.; He, C.; Hao, Z.; Chen, G. Comprehensive review on catalytic degradation of Cl-VOCs under the practical application conditions. *Crit. Rev. Environ. Sci. Technol.* **2020**, *52*, 311–355. [CrossRef]
104. Liao, Y.; Zhang, X.; Peng, R.; Zhao, M.; Ye, D. Catalytic properties of manganese oxide polyhedra with hollow and solid morphologies in toluene removal. *Appl. Surf. Sci.* **2017**, *405*, 20–28. [CrossRef]
105. Yang, W.; Peng, Y.; Wang, Y.; Wang, Y.; Liu, H.; Su, Z.; Yang, W.; Chen, J.; Si, W.; Li, J. Controllable redox-induced in-situ growth of MnO_2 over Mn_2O_3 for toluene oxidation: Active heterostructure interfaces. *Appl. Catal. B Environ.* **2020**, *278*, 119279. [CrossRef]
106. Su, Z.; Si, W.; Liu, H.; Xiong, S.; Chu, X.; Yang, W.; Peng, Y.; Chen, J.; Cao, X.; Li, J. Boosting the Catalytic Performance of CeO_2 in Toluene Combustion via the Ce-Ce Homogeneous Interface. *Environ. Sci. Technol.* **2021**, *55*, 12630–12639. [CrossRef]
107. Liu, H.; Chen, J.; Wang, Y.; Yin, R.; Yang, W.; Wang, G.; Si, W.; Peng, Y.; Li, J. Interaction Mechanism for Simultaneous Elimination of Nitrogen Oxides and Toluene over the Bifunctional CeO_2–TiO_2 Mixed Oxide Catalyst. *Environ. Sci. Technol.* **2022**, *56*, 4467–4476. [CrossRef]
108. Lu, P.; Ye, L.; Yan, X.; Chen, D.; Chen, D.; Chen, X.; Fang, P.; Cen, C. Performance of toluene oxidation over MnCe/HZSM-5 catalyst with the addition of NO and NH3. *Appl. Surf. Sci.* **2021**, *567*, 150836. [CrossRef]
109. Zhao, L.; Huang, Y.; Zhang, J.; Jiang, L.; Wang, Y. Al_2O_3-modified CuO-CeO_2 catalyst for simultaneous removal of NO and toluene at wide temperature range. *Chem. Eng. J.* **2020**, *397*, 125419. [CrossRef]
110. Xiao, G.; Guo, Z.; Li, J.; Du, Y.; Zhang, Y.; Xiong, T.; Lin, B.; Fu, M.; Ye, D.; Hu, Y. Insights into the effect of flue gas on synergistic elimination of toluene and NO over V_2O_5-$MoO_3(WO_3)/TiO_2$ catalysts. *Chem. Eng. J.* **2022**, *435*, 134914. [CrossRef]
111. Liu, L.; Shen, B.; Lu, F.; Peng, X. Highly efficient Mn-Fe bimetallic oxides for simultaneous oxidation of NO and toluene: Performance and mechanism. *Fuel* **2023**, *332*, 126143. [CrossRef]
112. Tang, J.; Zhao, L.; Jiang, S.; Huang, Y.; Zhang, J.; Li, J. Effect of Transition-Metal Oxide M (M = Co, Fe, and Mn) Modification on the Performance and Structure of Porous CuZrCe Catalysts for Simultaneous Removal of NO and Toluene at Low–Medium Temperatures. *Energy Fuels* **2022**, *36*, 4439–4455. [CrossRef]
113. Zhao, L.; Jiang, L.; Huang, Y.; Zhang, J.; Tang, J.; Li, C. Mechanism investigation of three-dimensional porous A-site substituted $La_{1-x}Co_xFeO_3$ catalysts for simultaneous oxidation of NO and toluene with H_2O. *Appl. Surf. Sci.* **2022**, *578*, 151977. [CrossRef]
114. Shao, J.; Wang, Z.; Liu, P.; Lin, F.; Zhu, Y.; He, Y.; Cen, K. Interplay effect on simultaneous catalytic oxidation of NO and toluene over different crystal types of MnO_2 catalysts. *Proc. Combust. Inst.* **2021**, *38*, 5433–5441. [CrossRef]
115. Yang, S.; Xiong, S.; Liao, Y.; Xiao, X.; Qi, F.; Peng, Y.; Fu, Y.; Shan, W.; Li, J. Mechanism of N_2O formation during the low-temperature selective catalytic reduction of NO with NH_3 over Mn-Fe spinel. *Environ. Sci. Technol.* **2014**, *48*, 10354–10362. [CrossRef]
116. Chen, S.; Vasiliades, M.; Yan, Q.; Yang, G.; Du, X.; Zhang, C.; Li, Y.; Zhu, T.; Wang, Q.; Efstathiou, A.M. Remarkable N_2-selectivity enhancement of practical NH_3-SCR over $Co_{0.5}Mn_1Fe_{0.25}Al_{0.75}O_x$-LDO: The role of Co investigated by transient kinetic and DFT mechanistic studies. *Appl. Catal. B: Environ.* **2020**, *277*, 119186. [CrossRef]
117. Han, L.; Cai, S.; Gao, M.; Hasegawa, J.; Wang, P.; Zhang, J.; Shi, L.; Zhang, D. Selective Catalytic Reduction of NO_x with NH_3 by Using Novel Catalysts: State of the Art and Future Prospects. *Chem. Rev.* **2019**, *119*, 10916–10976. [CrossRef]
118. Lu, P.; Ye, L.; Yan, X.; Chen, X.; Fang, P.; Chen, D.; Chen, D.; Cen, C. N_2O inhibition by toluene over Mn-Fe spinel SCR catalyst. *J. Hazard. Mater.* **2021**, *414*, 125468. [CrossRef]
119. Ye, L.; Lu, P.; Chen, X.; Fang, P.; Peng, Y.; Li, J.; Huang, H. The deactivation mechanism of toluene on MnO_x-CeO_2 SCR catalyst. *Appl. Catal. B: Environ.* **2020**, *277*, 119257. [CrossRef]